minerals

MDPI

Article

Albite ± Actinolite-Altered Porphyry Dykes in Archean Gold Deposits of the Boulder Lefroy-Golden Mile Fault System, Yilgarn Craton, Western Australia: Petrography, Chronology, and Comparison to Canadian Albitites

Andreas G. Mueller [1,*], Neal J. McNaughton [2] and Janet R. Muhling [3]

[1] Centre for Exploration Targeting, School of Earth Sciences, The University of Western Australia, 35 Stirling Highway, Perth, WA 6000, Australia
[2] John de Laeter Centre for Isotope Research, Curtin University, Kent Street, Bentley, WA 6102, Australia; N.McNaughton@curtin.edu.au
[3] School of Earth Sciences, The University of Western Australia, 35 Stirling Highway, Perth, WA 6000, Australia; janet.muhling@uwa.edu.au
* Correspondence: andreasm@iinet.net.au

Abstract: The Boulder Lefroy-Golden Mile fault system in the Archean Yigarn Craton is the most productive gold-mineralized structure in Australia (>2300 t Au). The New Celebration deposit (51 t Au) is part of a group of hematite- and anhydrite-bearing mesothermal deposits and Fe-Cu-Au skarns associated with monzodiorite-tonalite intrusions in the strike-slip fault system. Ore-grade biotite-carbonate and late sericite-carbonate-alkali feldspar replacement is bound to the contacts of a felsic (low Cr, Ni, V) quartz-plagioclase porphyry dyke dated at 2676 ± 7 Ma. The sodic-potassic alteration of the felsic boudinaged dyke contrasts with the albite-actinolite alteration in the adjacent mafic (high Cr, Ni, V) plagioclase porphyry dated at 2662 ± 4 Ma, although both share the same sulfide-oxide assemblage: pyrite ± chalcopyrite, magnetite ± hematite. The younger porphyry locally crosscuts foliation and is bordered by post-kinematic actinolite-pyrite selvages overprinting talc-chlorite-phlogopite-dolomite schist. It contains auriferous pyrite (70 ppb Au; 610 ppb Ag) where sampled for zircon U-Pb chronology at +224 m elevation. Above the sample site, the dyke was mined as gold ore (1–6 g/t Au) at +300–350 m. Temperature estimates based on actinolite-albite pairs (300–350 °C) agree with the fluid inclusion trapping temperature of main-stage auriferous veins (330 ± 20 °C). These relationships are interpreted to indicate syn-mineralization emplacement. Gold-related albite-altered porphyry dykes (albitites) also occur in the world-class Hollinger-McIntyre (986 t Au) and Kerr Addison-Chesterville deposits (336 t Au), Abitibi greenstone belt, Canada.

Keywords: gold; mesothermal; monzodiorite; porphyry; albitite; intrusion-related

Citation: Mueller, A.G.; McNaughton, N.J.; Muhling, J.R. Albite ± Actinolite-Altered Porphyry Dykes in Archean Gold Deposits of the Boulder Lefroy-Golden Mile Fault System, Yilgarn Craton, Western Australia: Petrography, Chronology, and Comparison to Canadian Albitites. *Minerals* **2021**, *11*, 1288. https://doi.org/10.3390/min11111288

Academic Editors: Antonia Cepedal and Mercedes Fuertes-Fuente

Received: 9 October 2021
Accepted: 15 November 2021
Published: 19 November 2021

1. Introduction

Albite-altered porphyry dykes termed "albitites" are associated in space and time with Archean gold deposits in the Abitibi greenstone belt, Canada, most notably Hollinger-McIntyre (986 t Au; 1910–2018) at Timmins in the Destor-Porcupine fault zone, and Kerr Addison-Chesterville (336 t Au; 1930–1996) in the Larder Lake-Cadillac Fault [1–3]. In the Boulder Lefroy-Golden Mile fault system (>2300 t Au; 1893–2020), eastern Yilgarn Craton, Western Australia (Figure 1), albitite dykes occur in the feeder zone below the East Repulse deposit at Kambalda [4].

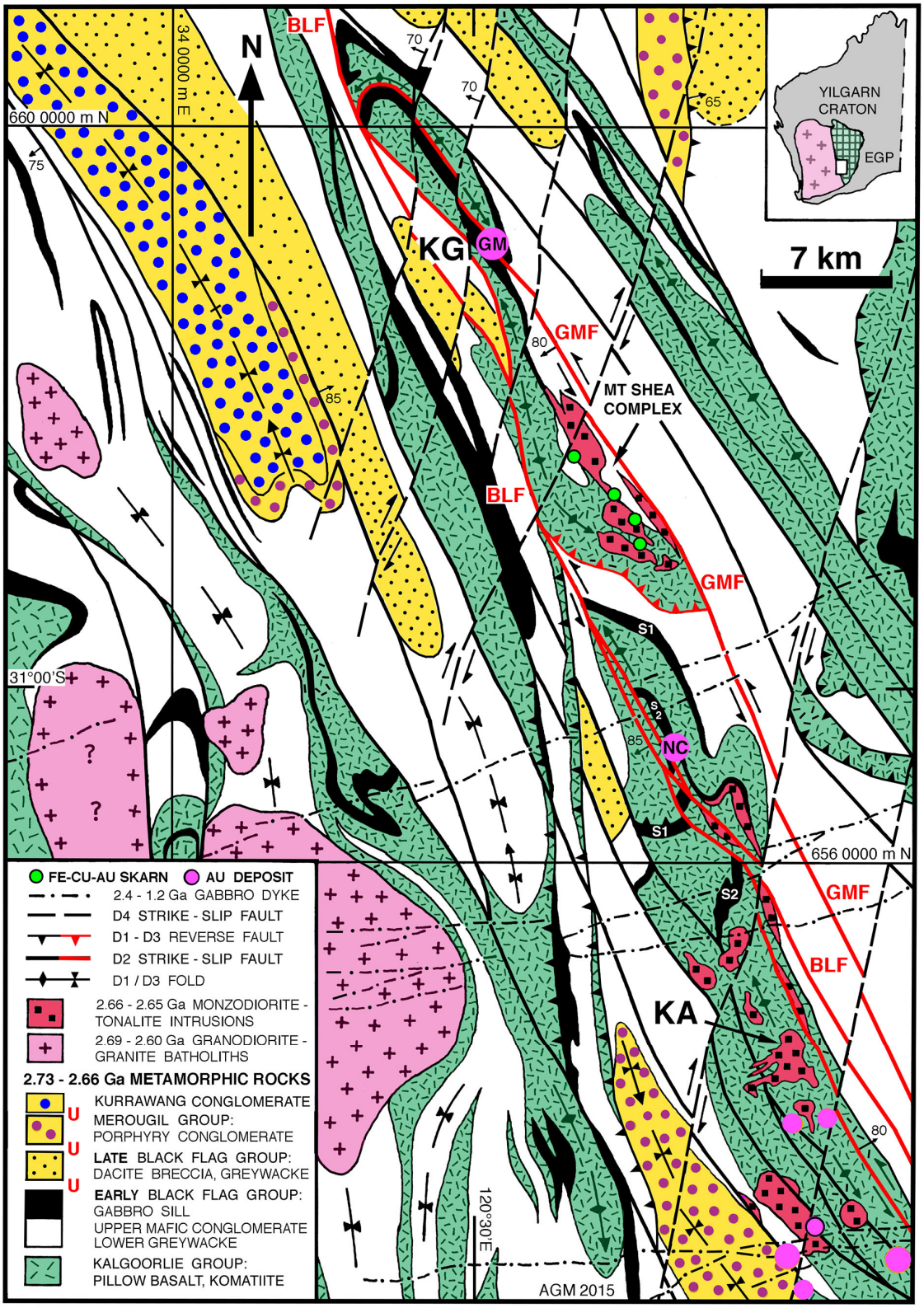

Figure 1. Geologic map of the southern Kalgoorlie Terrane showing the Boulder Lefroy-Golden Mile strike-slip fault system (BLF-GMF; in red), the folded stratigraphic units (U = unconformity) in the Kalgoorlie (KG)-Kambalda (KA) area, the locations of the Golden Mile (GM) and New Celebration (NC) mesothermal gold deposit, the Mt Shea monzodiorite-tonalite complex and associated Fe-Cu-Au skarns, and other gold deposits southeast of Kambalda (modified from [5]). Note the 12 km left lateral offset of metagabbro sills (S1; S2) at the Boulder Lefroy Fault. The UTM coordinates are Map Grid Australia (MGA) 1994, Zone 51. The inset of Western Australia shows the map area in the Eastern Goldfields Province (EGP) of the Yilgarn Craton.

We describe another occurrence in the Boulder Lefroy Fault, where hydrothermal albite in equilibrium with actinolite selectively overprints some dykes but not others in the porphyry swarm forming the New Celebration deposit (51 t Au; 1897–2009). Main-stage biotite- and late sericite-carbonate-pyrite mineralization is centered on a boudinaged porphyry dyke dated at 2676 ± 7 Ma (U-Pb zircon [5];). The weakly strained albite-actinolite altered porphyry northeast of the main dyke has been dated by a concordant U-Pb zircon age of 2662 ± 4 Ma (this study). It was mined as the B50 ore zone on the upper benches of the open pit [6] but has not been studied in detail given the absence of geochronology. We supplement our new U-Pb age with petrographic, mineralogical and geochemical data from the three main porphyry dykes in the deposit. The combined results suggest that gold mineralization took place during magmatic activity at 2662 ± 4 Ma.

We discuss the role of Mg-Na metasomatism in I-type monzodiorite-suite intrusions of sanukitoid-adakite affinity emplaced along the Boulder Lefroy-Golden Mile fault system at 2665–2655 Ma. We review the evidence for syn-mineralization dyke emplacement, first for the case studies at Kambalda and New Celebration, and then for albitites in major Canadian deposits. Our results suggest that the focus on regional faults alone is insufficient for the exploration of mesothermal gold deposits, and that high-Mg albite-altered dioritic intrusions must be considered for target selection.

2. Regional Geologic Setting

The Golden Mile (1790 t Au; 1893–2020) and New Celebration are part of a group of hematite-, anhydrite- and telluride-bearing mesothermal gold deposits, which cluster with associated porphyry stocks, dykes and Fe-Cu-Au skarns along the Boulder Lefroy-Golden Mile fault system in the Eastern Goldfields Province (EGP in Figure 1). The EGP in the Yilgarn Craton is a broad continental-margin orogen composed of 2.73–2.65 Ga greenstone belts and two major generations of granite batholiths (2.78–2.69 Ga; 2.68–2.60 Ga). The province is subdivided into the Kalgoorlie, Kurnalpi, and Burtville Terranes [7]. The greenschist to amphibolite facies metamorphic greenstones in the Kalgoorlie Terrane, an ensialic back-arc rift, consist of 5 km thick tholeiitic and high-Mg basalts marked by an extensive horizon of komatiite flows [5,8]. Greywacke turbidites, dacites, and polymictic conglomerates and sandstones overlie the mafic-ultramafic volcanic rocks (Figure 1).

Successive deformation phases (D1–D5) generated the following structures in the terrane, mainly during ENE-WSW shortening: D1 upright tight folds in the older mafic-ultramafic volcanic and greywacke successions; D2 sinistral strike-slip faults such as the Boulder Lefroy-Golden Mile system (Figure 1); D3 reverse faults in fault-block antiforms and tight synclines in the younger conglomerate-sandstone successions; D4 dextral strike-slip faults trending NNE; and D5 normal faults striking ENE [5].

Calc-alkaline hornblende monzodiorite-tonalite intrusions were emplaced into the Boulder Lefroy-Golden Mile fault system at 2665–2655 Ma during late D2 and early D3 [5,9,10]. Older dykes of quartz-plagioclase porphyry dated at ca. 2675 Ma are coincident with the younger ones in the Golden Mile at Kalgoorlie [11,12] and in the New Celebration deposit (this study). The stock-dyke complexes at Mt. Shea and Kambalda (Figure 1) contain zircon xenocrysts dated at 2677 ± 13 Ma and 2684 ± 4 Ma, respectively [5].

At Mt. Shea, Cu-Au epidote-magnetite endoskarns (0.27–0.56% Cu, 0.14–0.35 g/t Au, 2–6 g/t Ag) are controlled by D3 reverse faults transecting monzodiorite-tonalite stocks (Figure 1). Skarn assemblages and isotope data (pyrite $\delta^{34}S_{CDT}$ = 2.5‰, calcite $\delta^{13}C_{PDB}$ = − 5.3‰) indicate replacement at peak temperatures of 500 ± 50 °C by magmatic fluids. At the Shea prospect, actinolite and albite are major components of the skarn gangue. Retrograde sericite-chlorite-ankerite schist (up to 0.62% Cu, 1.6 g/t Au) above this ore body is linked to skarn formation by shared Ca-Fe-CO_2 metasomatism [10,13].

3. New Celebration Deposit Geology

The New Celebration deposit extends from the northern Hampton Boulder into the southern Jubilee lease (Figure 2a).

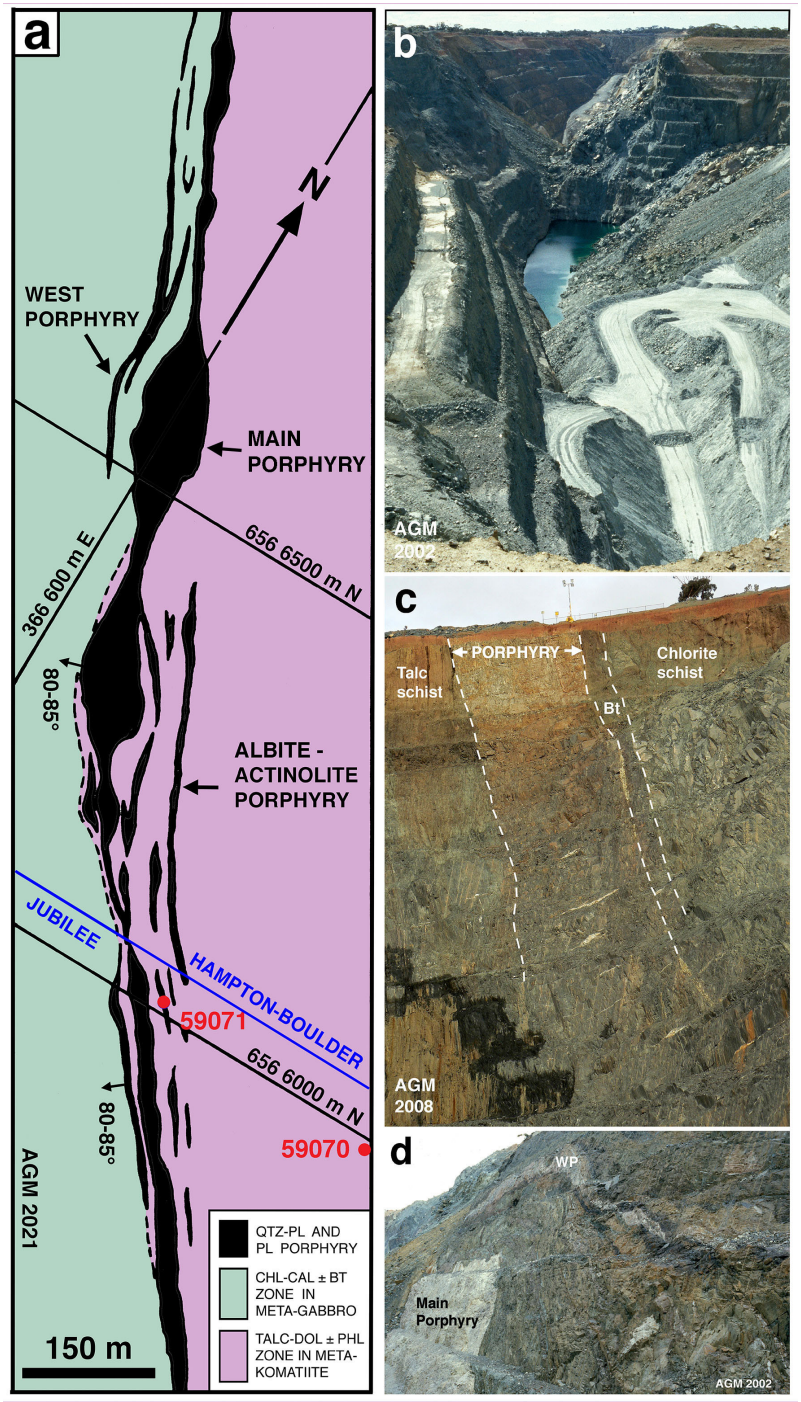

Figure 2. Porphyry dykes in the New Celebration gold deposit. (**a**) Map at 300 m above sea level showing the quartz-plagioclase (qtz-pl) and plagioclase porphyries at the contact of chlorite-calcite-biotite (chl-cal-bt) and talc-dolomite-phlogopite (talc-dol-phl) schist (modified from [14]). Surface samples 59070 and 59071 are projected. UTM coordinates are MGA 1994. (**b**) Looking N 35° W across the open pit in 2002. At the bench above the water table, the strike of the Boulder Lefroy Fault changes from N 40° W to N 15–20° W. (**c**) Looking SW at the wall of the Jubilee pit in 2008: the Main Porphyry separates chlorite-calcite schist and a biotite contact zone (Bt) from talc-dolomite schist. Flat quartz veins (white) link movement planes. (**d**) Looking south at the West Porphyry (WP) and brown biotite contact alteration (3–5 g/t Au) in chlorite-calcite schist, Hampton Boulder pit in 2002. The bench height is 10 m.

Underground production from the northern lease amounts to 0.893 million metric tons (Mt) at 7.83 g/t gold (1897–1996), and the combined open pit production to 20.3 Mt at 2.17 g/t (1986–2009). District-scale mapping [15] established that the deposit is located in the main branch of the Boulder Lefroy Fault. The correlation of meta-gabbro sills in the isoclinal D1 Celebration Anticline indicates 12 km of left-lateral offset (Figure 1). The main quartz-plagioclase porphyry dyke in the open pit, mineralized over a strike-length of more than 1 km, was boudinaged after emplacement at 2676 ± 7 Ma. The strain axes of boudins and necks plunge 69° NNW over a vertical distance of 140 m indicating slip along a line pitching 21° SSE [5], a transtensional setting coincident with the change in strike from N 15–20° W at Hampton Boulder to N 40° W at Jubilee (Figure 2a,b). In the open pit, stretching lineations pitching ±25° SE on talc-phlogopite foliation planes and asymmetric competent blocks are preserved in altered schist zones several meters thick [16–18], consistent with alteration during D2 sinistral oblique-slip.

Intercalated with these zones are others marked by steeply pitching lineations, flat quartz extension veins (Figure 2c), and shallowly plunging boudin axes in thin porphyry dykes. Locally, barren reverse faults (dip 40–50° SW or NE) of small offset displace the S2 foliation [16,17,19]. A gold quartz vein (dip 15° E), mined in high-Mg amphibolite 400 m east of the New Celebration pit, was dragged upward at the contact with sheared meta-komatiite [20]. These reverse structures have been interpreted to predate strike-slip [17], but probably result from ENE-WSW directed D3 shortening. They suggest that gold mineralization at New Celebration took place during the transition from D2 to D3, in analogy with time relationships documented in the Golden Mile deposit [12]. Post-D3 NNE- and ENE-striking faults are barren at New Celebration [17].

Wall-Rock Alteration

The gabbro sills, basalts, and komatiites in the Celebration Anticline were metamorphosed to lower amphibolite-facies assemblages of hornblende-epidote-albite and amphibole-chlorite, respectively, during regional D1 folding [5,21]. The boudinaged porphyry and adjacent dykes marking the D2 Boulder Lefroy Fault outcropped at surface, and fresh rock containing pyrite was encountered in shafts at 15–30 m depth [20]. Open pit mining since 1986 exposed a zone of retrograde schists more than 200 m wide, which includes lenses of meta-gabbro and meta-komatiite southwest and northeast of the dyke swarm, respectively [6]. The outer schists consist of mafic chlorite-calcite-albite and ultramafic talc-dolomite-chlorite assemblages (Figure 2c,d). The host rock alteration zones, not part of our porphyry study, are summarized in Figure 3. In all rocks, biotite-phlogopite and magnetite + pyrite characterize early-stage alteration, whereas sericite, chlorite (after biotite) and pyrite ± hematite characterize late-stage alteration. Limited electron microprobe analyses indicate that most of the "sericite" is phengite [22].

In the outer schists, biotite-phlogopite, magnetite and minor pyrite are concentrated in spaced, foliation-parallel bands increasing in abundance towards the porphyry contacts. Gold grades are low (0.05–0.26 g/t Au). At the boudinaged porphyry dyke, biotite-ankerite-albite + K-feldspar contact zones (Figure 2c,d) containing 10–15% magnetite + pyrite form the low-grade ore (2–5 g/t Au) mined in the open pit. Quartz-ankerite ± dolomite crackle veins straddle the dyke contacts and extend into the porphyry. Pyrite-rich sericitic vein selvages and zones may be subdivided into oxidized hematite-stained K-feldspar-albite-ankerite-phengite and reduced phengite-quartz-albite assemblages with rare hematite overprinting the early biotite alteration. Late-stage replacement formed high-grade ore shoots (8–10 g/t Au) mined underground in mafic contact schist [16]. In late ore, pyrite is dominant (5–15 vol.%), whereas magnetite is absent or remnant in pyrite. Native gold and tellurides (calaverite, petzite, hessite, melonite, altaite) form inclusions in pyrite and grains attached to its surface, associated with accessory chalcopyrite, galena, and barite [18]. Flat quartz-carbonate veins related to D3 reverse movement contain either biotite or phengite ± chlorite.

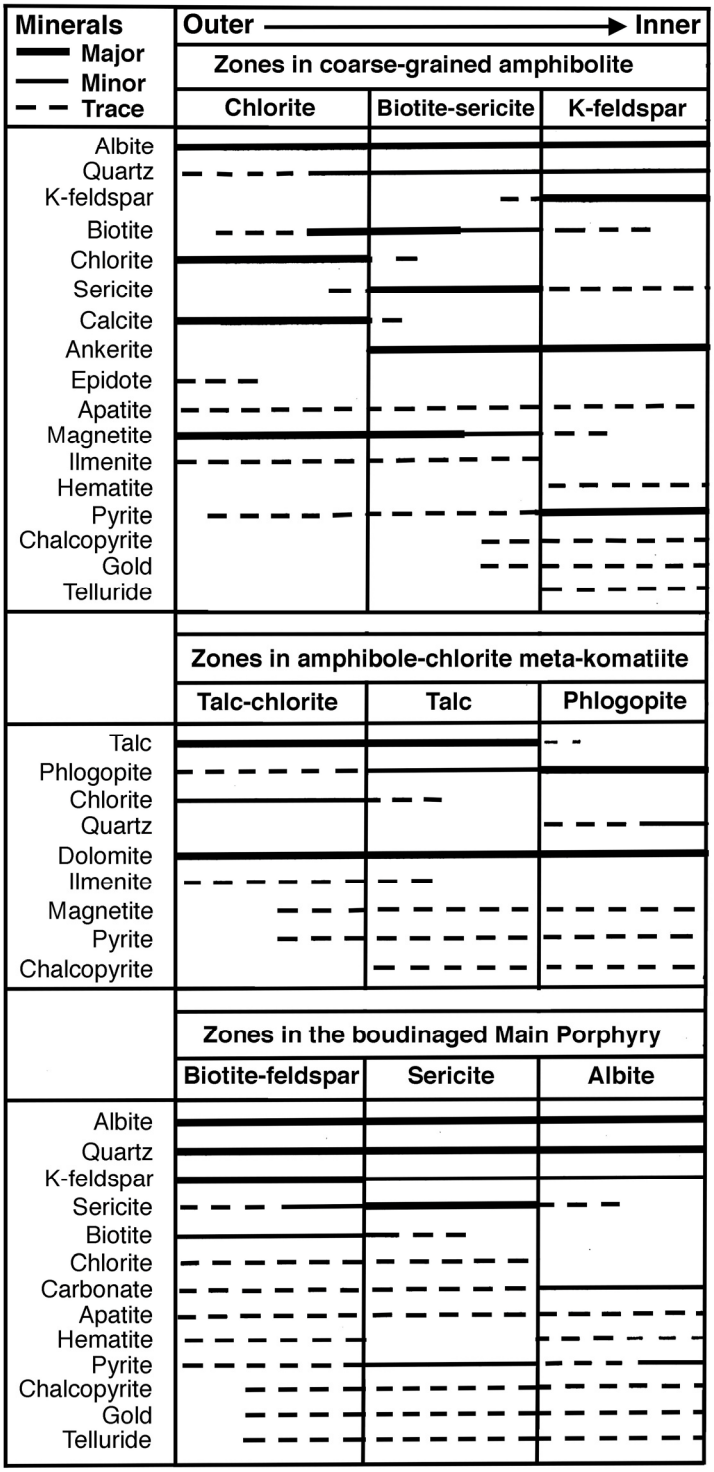

Figure 3. Paragenetic diagram of the main hydrothermal alteration zones in the three principal host rocks of the New Celebration gold deposit; compiled and modified according to own observations from data in [16,18,22].

A sulfur isotope study of pyrite gave positive $\delta^{34}S$ values (+3.92 to +5.54, n = 2) in magnetite-mineralized outer schist, and negative values (−1.41 to −8.64, n = 6) in hematite-stained porphyry and its SW-contact zone [23]. Though limited, the data indicate an increase in fluid oxidation state with time, and sulfur isotope fractionation between pyrite and co-genetic sulfate [24], probably anhydrite apart from the accessory barite.

The pressure-temperature conditions of main-stage gold mineralization are constrained by mineral assemblages and fluid inclusions in six quartz-carbonate veins with alkali feldspar-biotite-ankerite-pyrite replacement selvages [22]. Phengite (Si^{IV} = 3.233–3.351; Fe2 = 0.211–0.256; Mg = 0.163–0.247) in equilibrium with K-feldspar + biotite + quartz gave a pressure estimate of 400 MPa (4 kbar) using the calibration in [25] and assuming $P_{Total} = P_{H2O}$, a minimum at $X_{CO2} \geq 0.18$ in the fluid phase. The fluid inclusions were of low salinity (1.0–5.7 wt.% $NaCl_{eq}$), high bulk density (0.80–1.03 g/cc), and homogenized to both liquid and vapor at T_h = 300–370 °C indicating trapping in the 2-phase field ($T_h = T_{trapping}$). At a mean temperature of 330 ± 20 °C, bulk density isochores gave pressure estimates of 300–420 MPa [22], consistent with a mid-crustal level of 10–14 km depth for gold mineralization in the Boulder Lefroy-Golden Mile fault system [5].

4. Materials and Methods

In July 2008, the senior author collected petrographic, geochemical, and bulk samples for zircon and titanite separation (3–10 kg) from the boudinaged Main Porphyry (samples HB-5; HB-6), the Albite-Actinolite Porphyry (HB-3; HB-8a) and its 2–5 cm wide contact replacement selvage (HB-2; HB-9), a thin parallel albite-actinolite altered dyke (HB-8b), and the least-altered East Porphyry (HB-4; Figure 4) supplemented by background samples of talc-chlorite-dolomite schist and biotite-altered amphibolite. The sample coordinates were established by GPS survey. In early 2009, the talc schist forming the eastern pit wall collapsed causing the termination of mining.

Polished hand specimens were studied at low magnification (60×) under a Bausch & Lomb microscope (Laval, Canada), and polished thin sections (n = 14) in transmitted and reflected light using a Zeiss Universal microscope (Jena, Germany). Mineral identification was according to optical properties tabled in [26–28]. Two porphyry samples collected at surface in 1966 [29] were also re-examined and re-analyzed (University of Western Australia; UWA museum nos. 59070 and 59071; Figure 2).

Whole-rock samples were analyzed at Intertek/Genalysis (Perth, Australia) for major oxides and sulfur by X-ray Fluorescence (XRF) spectrometry, and for trace elements by Inductively Coupled Plasma Optical Emission (ICP-OES) or Mass Spectrometry (ICP-MS) using 4-acid digest or dissolution after lithium borate fusion. Gold, platinum and palladium were analyzed by fire assay. The chemical data, methods and detection limits are listed in Table S1 of the Supplementary Material together with background values for Neoarchean crust represented by trondhjemite-tonalite-granodiorite (TTG) batholiths, and with data for Archean adakites/sanukitoids of quartz monzodiorite composition [30,31]. Background values for average continental crust [32] are tabled where TTG-data are missing. Mesonorm mineral modes after [33] were calculated to allow comparison with the modal mineralogy observed in thin section. A pyrite concentrate from the Albite-Actinolite Porphyry, hand picked to >95% purity, was dissolved in aqua regia and analyzed by ICP-MS for selected trace elements.

Amphibole-plagioclase pairs in carbon-coated polished thin sections from the Albite-Actinolite Porphyry and the second quartz-actinolite veined dyke (samples HB-8a and HB-8b; Figure 4) were analyzed using an Oxford Instruments X-Max50 Energy Dispersive X-ray detector (EDS) mounted on a TESCAN Vega3 scanning electron microscope (SEM) at the Centre for Microscopy, Characterisation and Analysis at the University of Western Australia. The AZtec software from Oxford Instruments was used to process the spectra. Quantitative analyses were collected at 15 kV accelerating voltage and 1–2 nA beam current after calibrating the count rate on pure copper. The computer program AX was used for Fe^{3+}/Fe^{2+} allocation [34,35]. The data and analytical details are listed in Table S2.

Bulk samples for geochronology were crushed and ground to fine sand size, and the zircons concentrated using the Wilfley shaking table, lithium poly-tungstate heavy liquid, and the Frantz magnetic separator. Zircons were hand picked from the non-magnetic fraction, mounted in epoxy discs, polished and coated, and imaged in the SEM (Figure S1) prior to analysis in the Sensitive High Mass Resolution Ion Microprobe (SHRIMP II) at the

John de Laeter Center, Curtin University (Perth, Australia). The analytical procedures are reviewed in [36]. The U-Pb data of zircons from the Albite-Actinolite Porphyry are listed in Table S3. The program Isoplot/Ex 3.75 [37] was used to calculate ages and construct Concordia diagrams. All U-Pb ages are quoted at the 95% confidence level (2σ). Two fractions of hydrothermal titanite (2–6 ppm U; 10–15 ppm Pb) from this porphyry, analyzed commercially by Thermal Ionization Mass Spectrometry (TIMS) had low $^{206}Pb/^{204}Pb$ ratios of 20–35 making it impossible to calculate reliable ages due to the influence of the common lead correction.

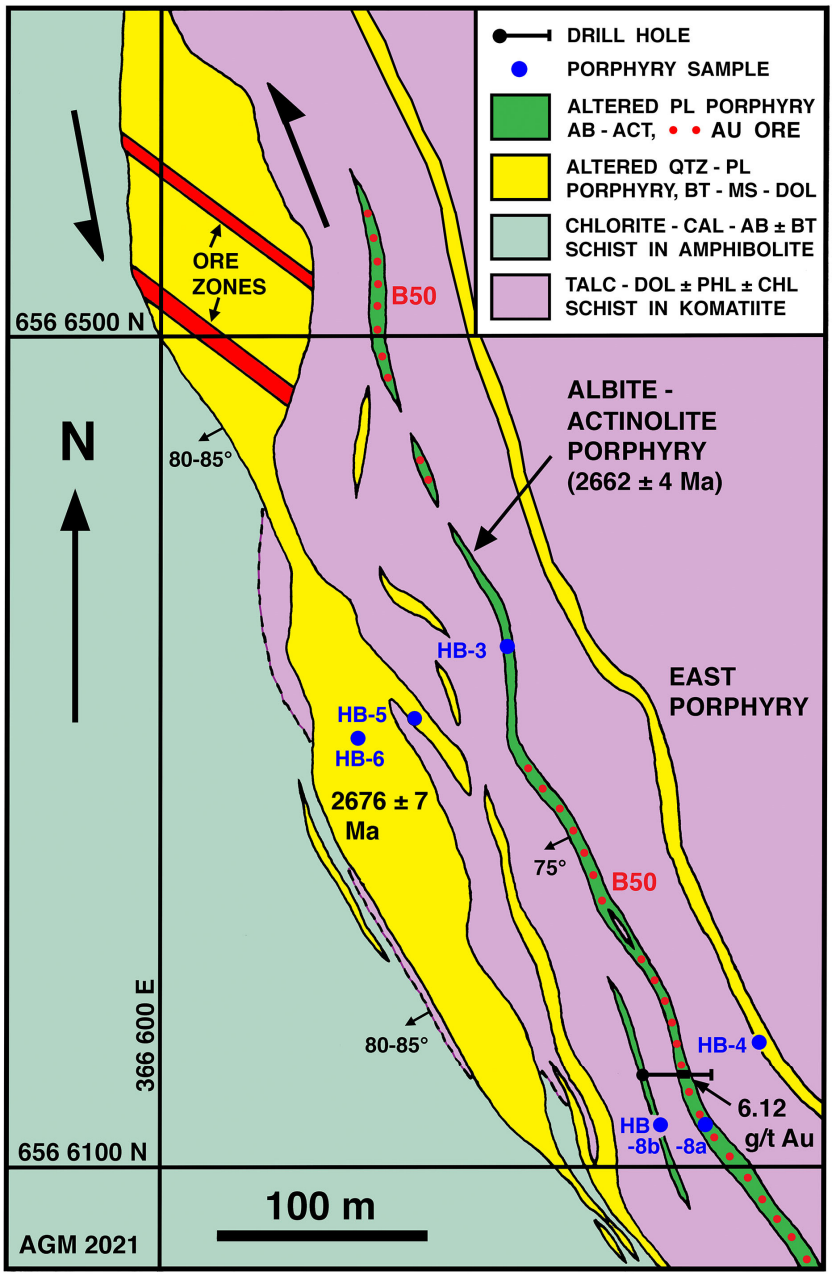

Figure 4. Surface geologic map (+355 m) of the Hampton Boulder part of the New Celebration deposit (modified from [38]) showing the porphyry dykes dated using zircons from samples HB-5 and HB-8a. Gold ore is bound to the intrusive contacts of all dykes except the East Porphyry. Two steeply dipping ore zones crossing the northern boudin of the main dyke indicate sinistral movement. The B50 ore zone and gold grade in the Albite-Actinolite Porphyry are from [6]. Minerals: actinolite (act), albite (ab), calcite (cal), chlorite (chl), dolomite (dol), phlogopite (phl), plagioclase (pl), pyrite (py), quartz (qtz). The UTM coordinates are MGA 1994.

5. Results

In the petrographic section below, geochemical data related to gold mineralization are emphasized. Trace elements patterns (Cr, Ni, V, Pt, Pd; Table S1) diagnostic of the crust or mantle provenance of the porphyry melts are evaluated in the Discussion.

5.1. East Porphyry (ca. 2675 Ma)

The East Porphyry contains less than 0.3 g/t gold and represents the least-altered dyke exposed in the open pit (Figure 4). The grey porphyry consists of subhedral plagioclase (0.5–2.5 mm; 30–40 vol.%), embayed quartz (2–3%), and rare apatite phenocrysts set in a microcrystalline quartz-albite groundmass. Selvages of dispersed hematite surround veinlets of quartz, albite, minor phengite, and calcite (Figure 5a). Dark brown biotite (5–7%), calcite (2%), phengite (0.5–1%), magnetite, pyrite and rutile (0.5% each) line grain boundaries and fractures and form aggregates, some probably pseudomorphous after hornblende (Figure 5a–d).

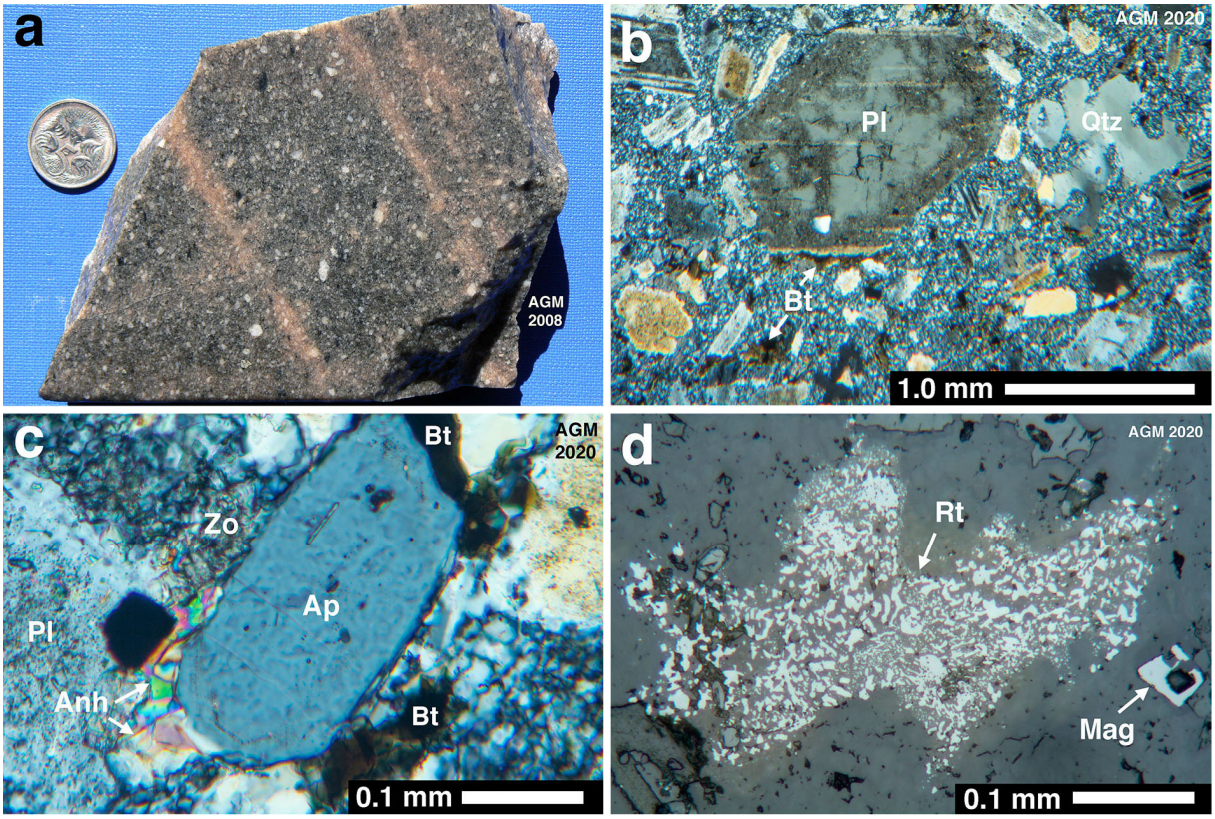

Figure 5. Photographs and photomicrographs of the East Porphyry, sample HB-4. (**a**) Quartz-plagioclase porphyry: white plagioclase glomerocrysts, quartz phenocrysts, and plagioclase laths in a microcrystalline groundmass. Brown biotite (7%) is disseminated and on fractures, and in biotite-calcite-phengite aggregates (after hornblende?). Red selvages of dispersed hematite surround quartz veinlets. The coin is 19 mm across. (**b**) Plagioclase (Pl) and embayed quartz (Qtz) phenocrysts are rimmed by biotite (Bt), calcite and zoisite, which also form aggregates in the groundmass. Crossed polarized light. (**c**) Apatite (Ap) and plagioclase phenocrysts (Pl) rimmed by oxidized biotite (Bt), anhydrite (Anh), zoisite (Zo), and opaque pyrite. Crossed polarized light. (**d**) Rutile (Rt) pseudomorphous after Ti-rich hornblende or pyroxene adjacent to magnetite (Mag). Plane polarized light reflected in air.

Trace amounts (0.5%) of actinolite, zoisite, and anhydrite (Figure 5c) replace plagioclase, whereas rutile locally outlines rare glomerocrysts of Ti-rich hornblende or pyroxene (Figure 5d).

The mineralogy is reflected in high normative albite (70%) and quartz (20%), minor biotite (4–5%) and calcite (4%), and low orthoclase (0.5%). Au, Ag, and Te are close to

background. Barium is high (1390 ppm) and the Rb/Sr ratio (0.01) extremely low (sample HB-4 in Table S1).

The quartz-plagioclase porphyry at the southeast margin of the open pit (59070; Figure 2) also has high normative albite (58%) and quartz (32%), no normative orthoclase but minor biotite (5%) and corundum (4%), the non-allocated Al_2O_3 probably reflecting phengite. Barium is high (1610 ppm) and the Rb/Sr ratio extremely low (<0.01). Ag (1.2 ppm), Te (0.7 ppm), Bi (4.0 ppm), and Pb (275 ppm) are enriched above background (Table S1).

5.2. Main Porphyry (2676 ± 7 Ma)

Mineralization extends from the contact ore zones into the interior of the boudinaged Main Porphyry. Close to the contact, dispersed hematite stains the K-feldspar-albite groundmass of early biotite alteration (Figure 6a), and the sericitic selvages of late crackle veins (Figure 6b), where biotite is selectively replaced by phengite + ankerite ± chlorite and magnetite by pyrite. Pheno- and glomerocrysts of twinned plagioclase (0.5–3 mm; 20–30 vol.%) and of embayed quartz (0.3–2 mm; 2–3%) define the porphyritic texture. Most plagioclase glomerocrysts are partly replaced by microcline, mainly along the margin and in domains crosscutting albite twins. Aggregates of fine-grained biotite and ankerite, some pseudomorphous after hornblende (Figure 6c) contain accessory Mg-Fe chlorite, rutile, magnetite, pyrite, and chalcopyrite (Figure 6d).

The main Mesonorm minerals are albite (54%), quartz (19%), and orthoclase (16%; HB-5 in Table S1) indicating more K-feldspar than detected microscopically, accompanied by minor carbonate (5%), biotite (4%) and phengite (1%, as corundum). Au (0.54 g/t), Ag (0.29 ppm) and Te (0.11 ppm) are enriched, barium (1672 ppm) is at the same level as in the least-altered sample HB-4, but the Rb/Sr ratio (0.04) is higher (Table S1).

In the center of the boudin, the alteration style controlled by crackle and shear fractures is texture-destructive, and higher in pyrite (5–10 vol.%) and carbonate content (10–15% Fe-dolomite ± ankerite). Magnetite is absent and red hematite stains are sparse. Plagioclase phenocrysts are largely replaced in sericite + quartz but partly preserved in feldspar-stable zones (Figure 6e), which contain alteration albite, untwinned K-feldspar and microcline. Native gold occurs enclosed in and attached to pyrite (Figure 6f). Veins are filled with quartz, minor albite and Fe-dolomite, and accessory phengite, apatite, pyrite, rare hematite, and tourmaline. Thicker veins (10 mm) have diffuse albite replacement selvages.

Although imprecise, the normative mineralogy of the strongly altered sample (HB-6 in Table S1) from the central part of the southern boudin (Figure 4) indicates abundant albite (55%) and carbonate (18%), and moderate amounts of quartz (8%), orthoclase (6%), and pyrite (4%). Most biotite (12%) is considered to represent phengite because of incorrectly allocated Mg + Fe, as the normative carbonate is calcite and not dolomite-ankerite. The sericite-altered porphyry has a high gold grade (11.2 g/t) and is enriched in Ag (1.53 ppm), Se (1.1 ppm), and Te (1.57 ppm).

5.3. Albite-Actinolite Porphyry (2662 ± 4 Ma)

The Albite-Actinolite Porphyry was sampled at two locations: (1) on the highest accessible bench in the NE-wall 267 m above sea level, and (2) on the pit floor at +224 m (Figure 4). On the Hampton Boulder lease, the dyke was mined as the B50 ore zone at a cut-off grade of 1.0 g/t gold from the surface at 355 m down to 300 m above sea level [6], 25–40 m below the oxidation zone. The only published grade is 6.12 g/t Au over 11 m in a drill hole at +325 m elevation above our sample site at +224 m (Figure 4).

On the +267 m bench, an in-situ segment of the dyke 1.5–2.0 m thick and oriented N 20° W/75° SW was exposed. The intrusive contact was locally discordant to the foliation in the host rock (Figure 7a), ultramafic talc-dolomite-phlogopite-chlorite schist mineralized with magnetite (2 vol.%), pyrite (1%) and chalcopyrite (0.3%). Fractures in the dyke were coated with talc. The porphyry contains rare amphibolite xenoliths, and 20–25 vol.% twinned plagioclase pheno- (0.25–1.2 mm) and glomerocrysts (1.5–4 mm) moderately

embayed by the pink, albite-rich groundmass (Figure 7b). Many are partly replaced by minor zoisite-sericite-calcite aggregates. Quartz phenocrysts are absent. Mafic aggregates (0.5–3 mm; 10%), some pseudomorphous after amphibole (Figure 7c,d), are composed of ankerite, white mica (phengite ± talc), titanite-rutile grains, magnetite, and pyrite. Aggregates (2%) of pyrite with chalcopyrite inclusions (Figure 7e) are in contact with subhedral magnetite (1%).

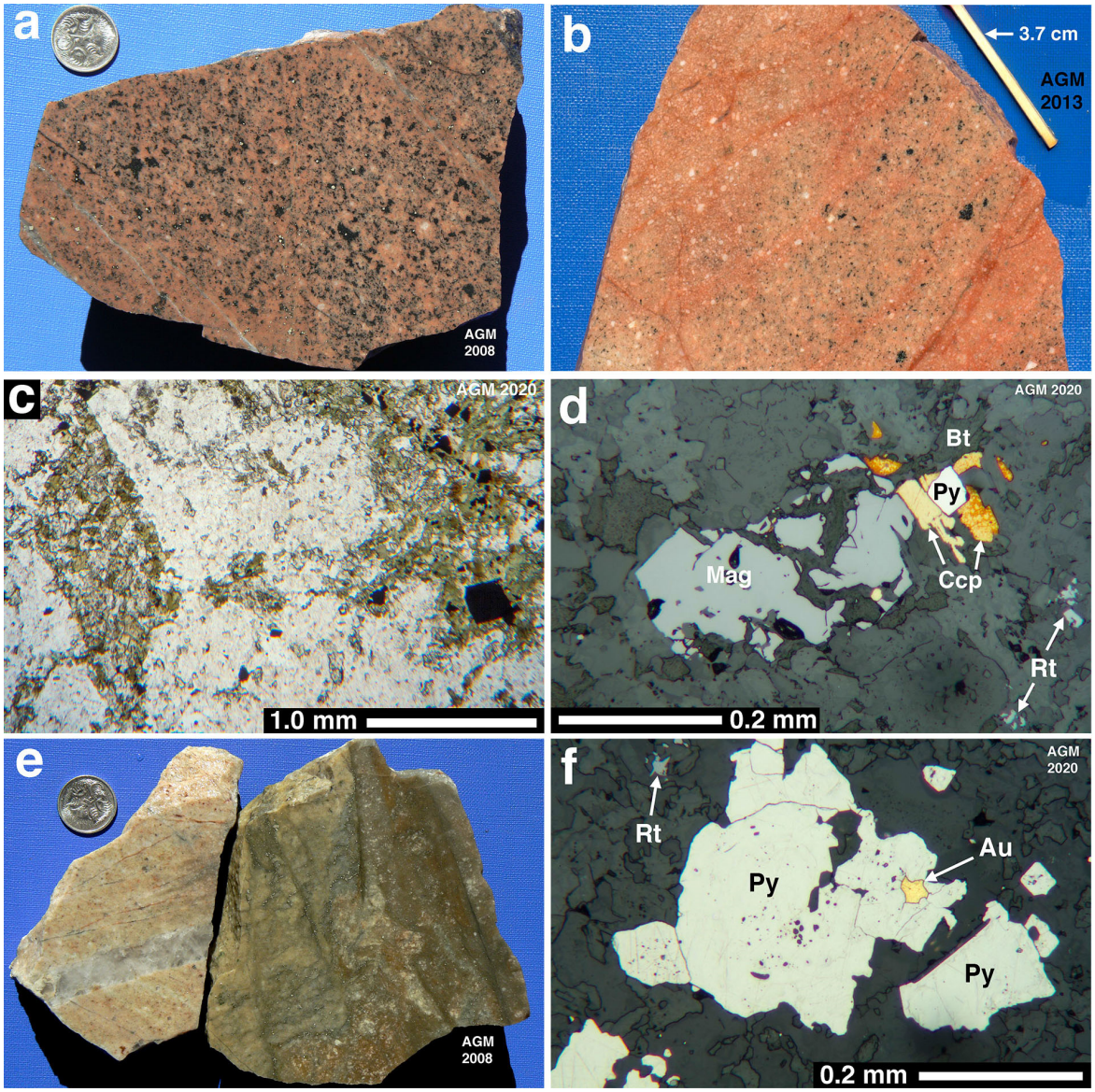

Figure 6. Photographs and photomicrographs of the boudinaged Main Porphyry, samples HB-5 (**a**–**d**) and HB-6 (**e**,**f**). (**a**) Early biotite alteration: white plagioclase phenocrysts are embayed by hematite-stained albite + K-feldspar ± quartz. Brown biotite, ankerite, magnetite, and pyrite form aggregates. The coin is 19 mm across. (**b**) Late sericite-hematite-pyrite alteration: white plagioclase phenocrysts are embayed by pink albite + K-feldspar ± quartz. In the red selvages of fractures, biotite is replaced by phengite + chlorite ± rutile and magnetite by pyrite. (**c**) Early biotite alteration: biotite + ankerite after rhomb-shaped hornblende adjacent to xenomorph biotite-ankerite and opaque magnetite-pyrite in an alkali feldspar groundmass. Plane polarized light. (**d**) Early biotite alteration: magnetite (Mag) in contact with biotite (Bt), chalcopyrite (Ccp), and pyrite (Py) adjacent to rutile (Rt). Plane polarized light reflected in air. (**e**) Late alteration. RIGHT: sericitic replacement, crackle fractures control phengite + pyrite in albite + dolomite + quartz. LEFT: albite-quartz-dolomite replacement centered on a quartz ± albite ± tourmaline vein. The coin is 19 mm across. (**f**) Late sericitic alteration: native gold (Au) enclosed in pyrite (Py) adjacent to rutile (Rt). Plane polarized light reflected in air.

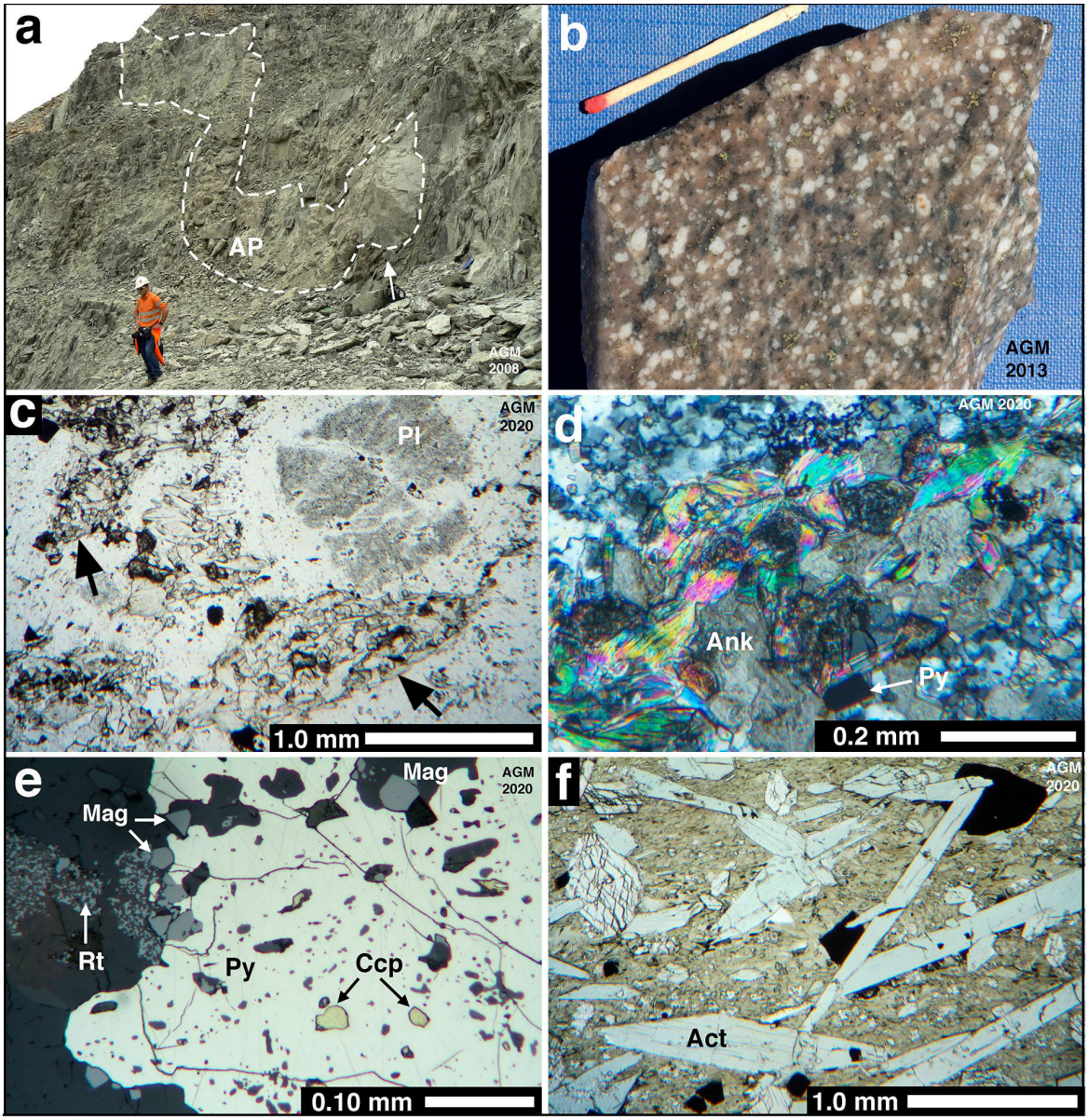

Figure 7. Photographs and photomicrographs of the Albite-Actinolite Porphyry: NE-wall of the open pit at +267 m, samples HB-3 (**a**–**e**; porphyry) and HB-2 (**f**; contact selvage). (**a**) Looking north at a section sub-parallel to strike through the porphyry dyke (AP; dashed line), the intrusive contact cuts across the foliation (arrow) in ultramafic schist. (**b**) White plagioclase phenocrysts in a pink albite-rich groundmass. Dark pseudomorphs after amphibole composed of ankerite, phengite, talc, pyrite (2 vol.%), magnetite (2%), and titanite-rutile (0.5–1%). The matchstick is 43 mm long. (**c**) Fractured plagioclase glomerocryst (Pl) and ankerite-phengite ± talc ± titanite-rutile ± pyrite aggregates after amphibole (arrows). Plane polarized light. (**d**) Phengite + ankerite (Ank) ± talc ± titanite-rutile ± pyrite (Py) aggregate after amphibole. Crossed polarized light. (**e**) Pyrite (Py) with chalcopyrite inclusions (Ccp) in contact with magnetite (Mag) and rutile (Rt). Plane polarized light reflected in air. (**f**) Replacement in talc-dolomite-chlorite schist: post-kinematic actinolite (Act), opaque magnetite, and pyrite in a phlogopite ± dolomite matrix. Plane polarized light.

While actinolite absent in the porphyry, actinolite-rich replacement about 5 cm wide marks the intrusive contact. Actinolite needles (0.5–5 mm; 35–50 vol.%) are randomly oriented in a matrix of phlogopite (10–40%), dolomite ± calcite (15–40%), and accessory Mg-rich chlorite (Figure 7f). The actinolite is in mutual contact with pyrite (1–5%), rare chalcopyrite (0.5%), and zoned magnetite (1–2%).

On the pit floor at +224 m, the Albite-Actinolite Porphyry was blasted and dismembered into boulders up to 2 m long. Felted actinolite needles formed a post-kinematic

replacement selvage (Figure 8a,b) in dolomite-banded talc-chlorite ± phlogopite schist. In the dyke, the porphyritic texture is caused by twinned plagioclase pheno- and glomerocrysts (0.25–4 mm; 20 vol.%) variably embayed by the dark grey albite-rich groundmass. The porphyry contains sparse xenoliths of fine-grained amphibolite, and rounded feldspar aggregates of uncertain origin (Figure 8c). In contrast to the upper bench, unaltered actinolite (0.1–1 mm; 20%), calcite, and dolomite (3–5%) are abundant in the groundmass locally replacing the margins of plagioclase phenocrysts (Figure 8d). Pyrite (3–5%) is evenly disseminated, in mutual contact with actinolite, and associated with chalcopyrite (0.2%), subhedral magnetite (0.5%), and aggregates of ilmenite (0.5–1%). Hematite (0.2%) rims most magnetite grains (Figure 8e), and forms domains in ilmenite (Figure 8f) indicating late oxidation.

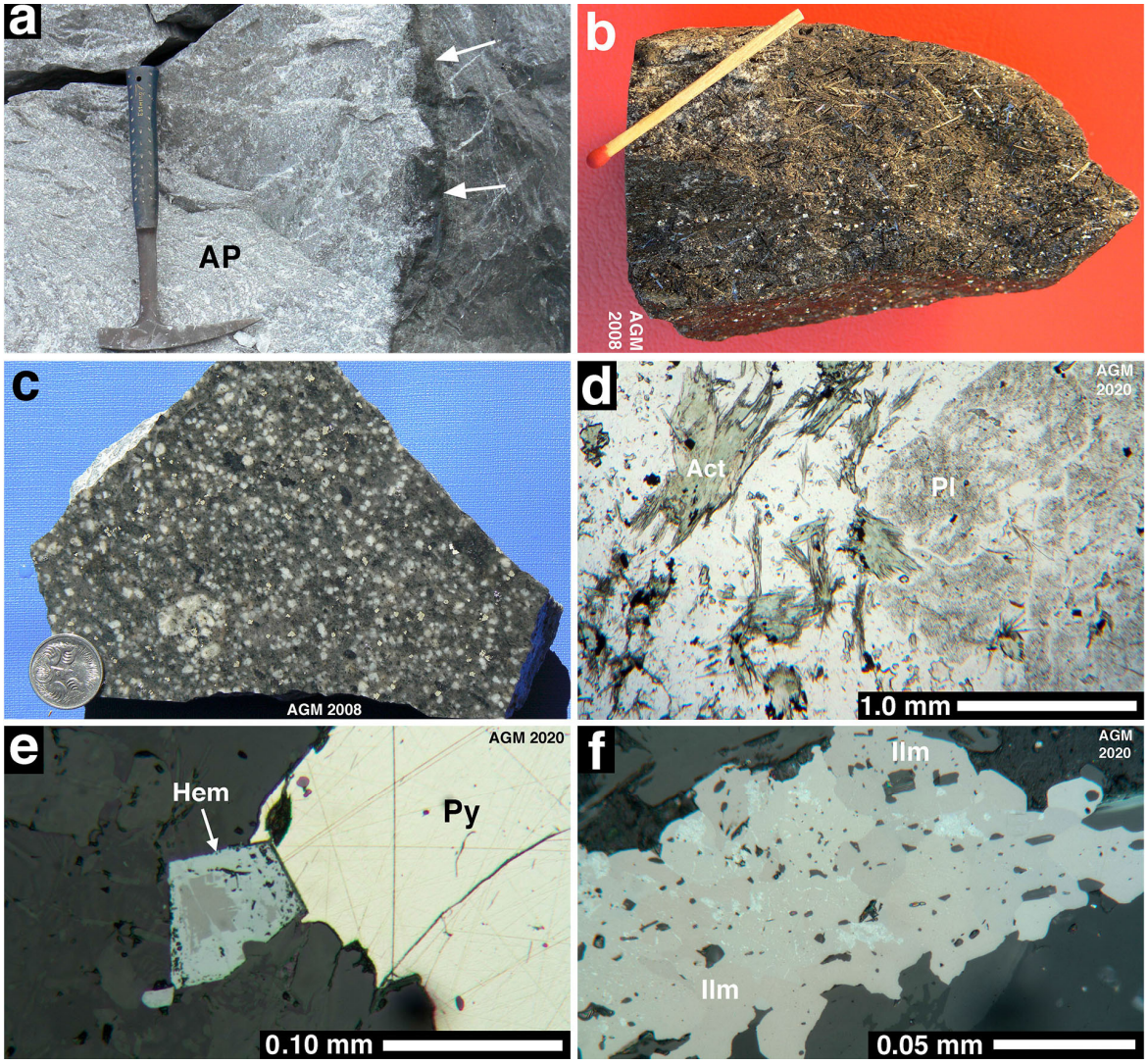

Figure 8. Photographs and photomicrographs of the Albite-Actinolite Porphyry: pit floor at 224 m above sea level, samples HB-8a and HB-9. (**a**) Altered Porphyry (AP), the post-kinematic contact selvage of black actinolite (arrows) overprints dolomite-veined talc–chlorite-phlogopite schist. The hammer is 32 cm tall. (**b**) Felted actinolite needles and cube-shaped pyrite in the contact selvage of the porphyry. The matchstick is 43 mm long. (**c**) Porphyry: white plagioclase pheno- and glomerocrysts and a rounded plagioclase aggregate in an albite-rich groundmass containing actinolite (15–20 vol.%), calcite (5%), pyrite (3–5%), and hematite (0.2%). The coin is 19 mm across. (**d**) Porphyry: plagioclase glomerocryst (Pl) partly replaced by actinolite (Act) and albite. Plane polarized light. (**e**) Porphyry: hematite (Hem) rims magnetite (brown core) in contact with pyrite (Py). Plane polarized light reflected in air. (**f**) Porphyry: aggregate of ilmenite (Ilm) with blue hematite domains of higher reflectance. Plane polarized light reflected in air.

The Mesonorm of sample HB-8a from the pit floor indicates high normative albite (76%) and calcic amphibole (16%), moderate carbonate (3–4%) and pyrite (3%), and accessory quartz (2%) and titanite (1%). The biotite content (4%) is incorrect due to Mg-allocation from dolomite, as the normative carbonate is calcite. The Mesonorm calculation for sample 59071 failed (Table S1). Biotite and K-feldspar are rare or absent given the low K_2O contents (0.08–0.11 wt.%). Both samples are also low in Ba (158–214 ppm). A pyrite concentrate from sample HB-8a was analyzed to compare chalcophile element enrichment to the pattern in main-stage gold ore. The pyrite in the porphyry contained 70 ppb gold, 610 ppb Ag, and elevated Bi, Cu, Mo, Pb, Se, and Te (Table 1).

Table 1. Trace element analyses of pyrite from the Albite-Actinolite Porphyry and of gold ore from the boudinaged Main Porphyry, New Celebration deposit.

Element	HB-8a Pyrite	HB-6 Gold Ore	Detection Limit in Pyrite
Ag (ppm)	0.61	1.53	0.05
As	36	1.1	1
Au	0.070	11.2	0.001
Bi	4.54	0.64	0.01
Cu	154	8.2	1
Hg	0.15	0.005	0.01
Mo	7.7	1.5	0.1
Pb	34.2	34	0.5
Sb	0.11	0.51	0.02
Se	13	1.1	1
Te	2.85	1.57	0.01
Zn	5	56	1

Handpicked pyrite concentrate (HB-8a), aqua regia digest, ICP-OES for Cu and Zn, ICP-MS for all other elements. Detection limits for sample HB-6 and background values are in Table S1b. Elements in bold are more than three-times the background in both HB-8a pyrite and HB-6 gold ore.

5.4. Temperature and Age Constraints

The temperature during sodic–calcic alteration in the Albite-Actinolite Porphyry and in the quartz-actinolite veined second dyke (samples Hb-8a and -8b in Figure 4) is constrained by the composition of the two main alteration minerals. All amphiboles are Mg-rich "actinolite" according to the classification of the International Mineralogical Association [39] given $Mg/(Mg+Fe^{2+}) = 0.77–0.85$, Si = 7.659–7.968 and Ca = 1.744–1.868. The associated plagioclase is pure albite (An1–2; Table S2). Empirical NaSi-CaAl exchange equilibria [40] indicate a temperature range of 300–350 °C (Figure 9a).

Except for a single xenocryst, the zircons recovered from the Albite-Actinolite Porphyry belong to a homogenous igneous population of bi-pyramidal, long prismatic, zoned crystals imaged in the Scanning Electron Microscope (Figure S1). The ion-microprobe spot analyses concordant in the U-Pb system are grouped into: (1) data from the xenocryst ($n = 4$; MSWD = 1.5) with a Th/U ratio of 0.99 and a weighted mean $^{207}Pb/^{206}Pb$ age of 2791 ± 29 Ma (2σ), probably inherited from basement granitoid, and (2) data from 15 igneous crystals ($n = 16$; MSWD = 1.14) with an average Th/U ratio of 0.70 and a weighted mean $^{207}Pb/^{206}Pb$ age of 2662 ± 4 Ma (Table S3). The U-Pb analyses of the second group are tightly clustered and overlap on Concordia within 1-sigma error (Figure 9b). Consequently, the age is interpreted to date dyke emplacement.

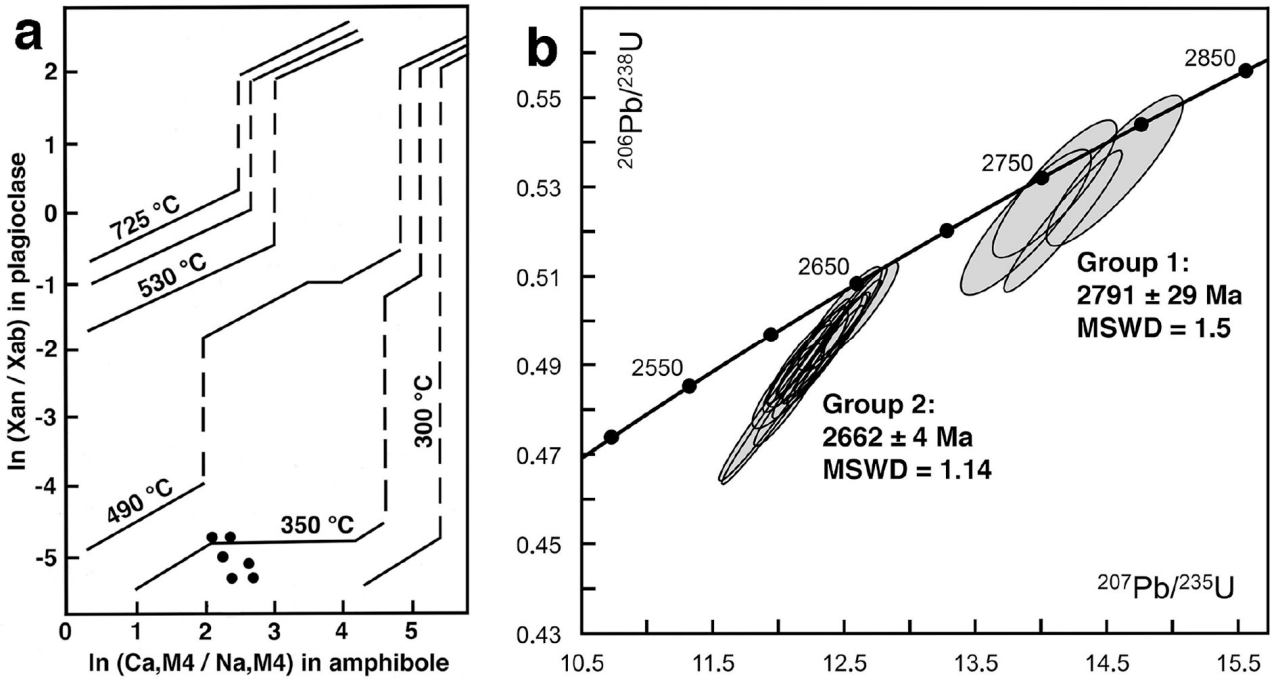

Figure 9. Temperature estimates and U-Pb zircon age of the Albite-Actinolite Porphyry. (**a**) Diagram showing the NaSi-CaAl exchange equilibria of ln(Xan/Xab) plagioclase and ln(Ca,M4/Na,M4) amphibole (after [40]). The mineral pairs (black dots) from albite-actinolite altered porphyries (samples HB-8a and -8b; Table S2) plot between the 300 °C and 350 °C contour lines (±25 °C). (**b**) U-Pb Concordia diagram of SHRIMP ion-microprobe spot analyses in zircons from the Albite-Actinolite Porphyry (sample HB-8a; Table S3). The concordant data (≤5% discordant) of the single xenocryst define a weighted mean $^{207}Pb/^{206}Pb$ age of 2791 ± 29 Ma (Group 1: n = 4), and those of igneous crystals a $^{207}Pb/^{206}Pb$ age of 2662 ± 4 Ma (Group 2: n = 16). The error ellipses are 1-sigma.

5.5. Classification of the Porphyry Suite

In the Albite-Actinolite Porphyry, igneous hornblende is absent, the shape of plagioclase pheno- and glomerocrysts is preserved, but internal oscillatory zones are not. The thin dyke to the southwest (sample HB-8b in Figure 4) contained quartz veins zoned to actinolite ± calcite margins (Figure 10a), fractures lined with actinolite, calcite and titanite (0.5 vol.%), disseminated pyrite (3%), and accessory (0.5–1%) biotite and Mg-Fe chlorite (Figure 10b).

In comparison, least-altered porphyry 750 m northeast of the open pit is composed of green hornblende (15 vol.%), zoned calcic plagioclase (25%; An15–20) and quartz phenocrysts (1%) set in a microcrystalline feldspar ± quartz groundmass, a composition close to quartz monzodiorite or diorite. Minor deuteric alteration (5% total) is evident in the local replacement of hornblende by actinolite, epidote and biotite, and of plagioclase by clinozoisite, sericite and albite (Figure 10c,d).

In the Pearce Zr/Ti versus Nb/Y diagram, designed to eliminate the effect of alteration [41], the porphyries plot in the sub-alkaline andesite and dacite-rhyolite fields (Figure 11a). The andesitic monzodiorite-suite porphyries at New Celebration also plot in the adakite field of the Sr/Y versus yttrium discrimination diagram, like their counterparts from Mt Shea and Kambalda (Figure 11b). The chondrite-normalized rare earth element (REE) patterns of all samples lack europium anomalies, and display depletion of the heavy relative to the light rare earths (Figure 11c), a feature interpreted to result from the fractional crystallization of hornblende, apatite, and titanite in hydrous calc-silicate melts [42].

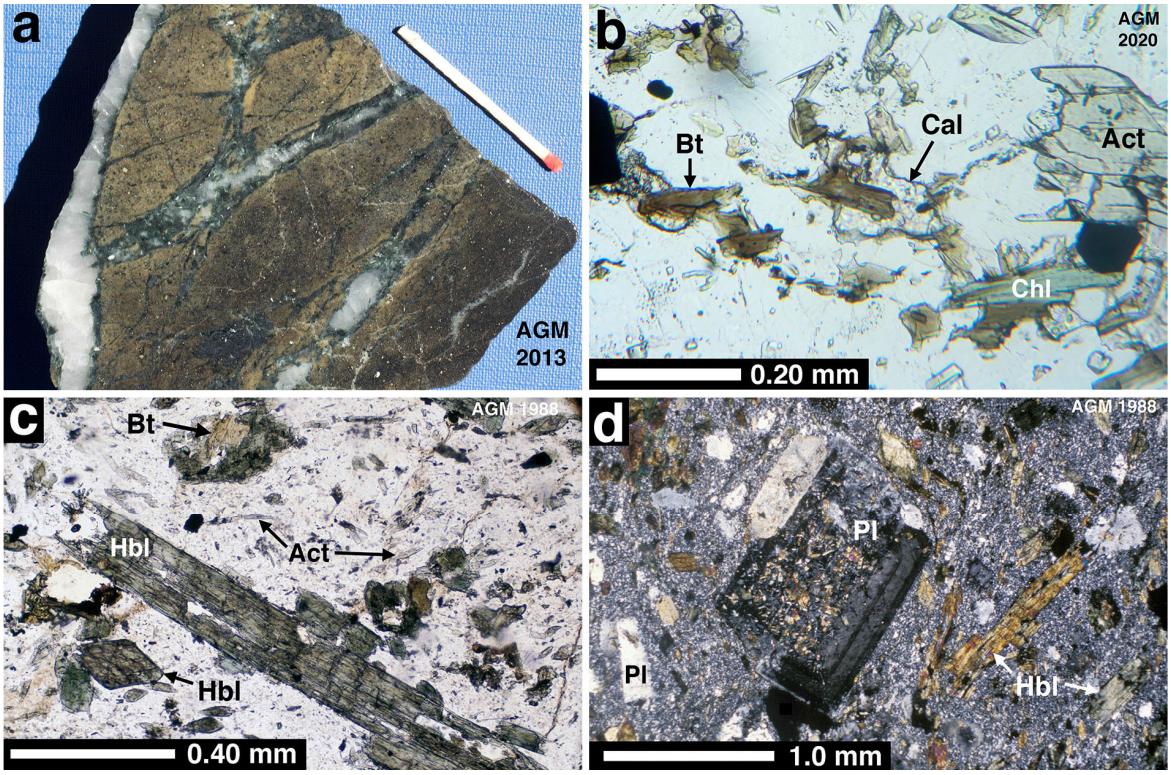

Figure 10. Photographs and photomicrographs of the second albite-actinolite altered dyke (**a**,**b**; sample HB-8b in Figure 4) and of least-altered quartz monzodiorite or diorite porphyry 750 m northeast of New Celebration (**c**,**d**; UWA no. 59072). (**a**) Zoned quartz-actinolite veins and fractures lined with green actinolite, calcite, and titanite crosscut an aphanitic albite groundmass containing pyrite (5 vol.%), biotite (1%), rutile and hematite (0.5%). The matchstick is 43 mm long. (**b**) Actinolite (Act), biotite (Bt), and Mg-Fe chlorite (Chl) in contact with calcite (Cal) and opaque pyrite in albite-rich groundmass. Plane polarized light. (**c**) Igneous green hornblende pheno- and glomerocrysts (Hbl), locally rimmed by brown biotite (Bt), in a feldspar ± quartz groundmass containing acicular actinolite (Act). Plane polarized light. (**d**) Igneous hornblende phenocrysts (Hbl) and plagioclase pheno- and glomerocrysts (Pl), some with oscillatory compositional zones partly replaced by clinozoisite and sericite. Crossed polarized light.

6. Discussion

We discuss the petrographic classification of the New Celebration porphyries first followed by a review of Mg-Na enrichment in calc-alkaline monzodiorite-suite intrusions emplaced into the Boulder Lefroy-Golden Mile fault system, a trend probably including "albitites" as the hydrothermal end member. We then assess the time relationship of albite-altered porphyries to gold mineralization in the East Repulse ore body at Kambalda and at New Celebration. This assessment is extended to albitite dykes in gold deposits controlled by regional fault zones in the Abitibi greenstone belt, Canada.

6.1. Older Porphyry Suite (ca. 2675 Ma)

The dacitic quartz-plagioclase porphyries at New Celebration (Figure 11a) are interpreted as fractionated members of the I-type trondhjemite-tonalite-granodiorite (TTG) suite common in Neoarchean batholiths [30,31]. In the ensialic Kalgoorlie Terrane of the continental-margin Eastern Goldfields fold belt, these batholiths have a significant monzogranite component [43]. In plutonic terms, the boudinaged Main Porphyry (2676 ± 7 Ma) and the East Porphyry represent granodiorite or tonalite differentiated due to hornblende fractionation. The extreme depletion of the heavy REE (normalized La/Yb = 83–85; Table S1) suggests melt equilibration with a garnet-bearing restite in the source region of the calc-alkaline magma [43]. The TiO_2 (0.17–0.24 wt.%), Cr (11–22 ppm), Ni (2–10 ppm) and V (16–20 ppm) values of these porphyries are below the average of TTG-batholiths

(Table S1), parameters also suggesting evolved melts. Platinum and palladium are below detection (<1 ppb). The exception is sample HB-6, which plots in the andesite and adakite fields (Figure 11a,b) and has elevated Cr (141 ppm), Ni (73 ppm), V (39 ppm), Pt (4 ppb), and Pd (3 ppb). For this gold-rich sample, a mixed heritage is possible as a late dyke was observed underground to crosscut quartz-plagioclase porphyry in the southern boudin of the main dyke [16], a position close to where bulk sample HB-6 was collected from the blast pile on the pit floor.

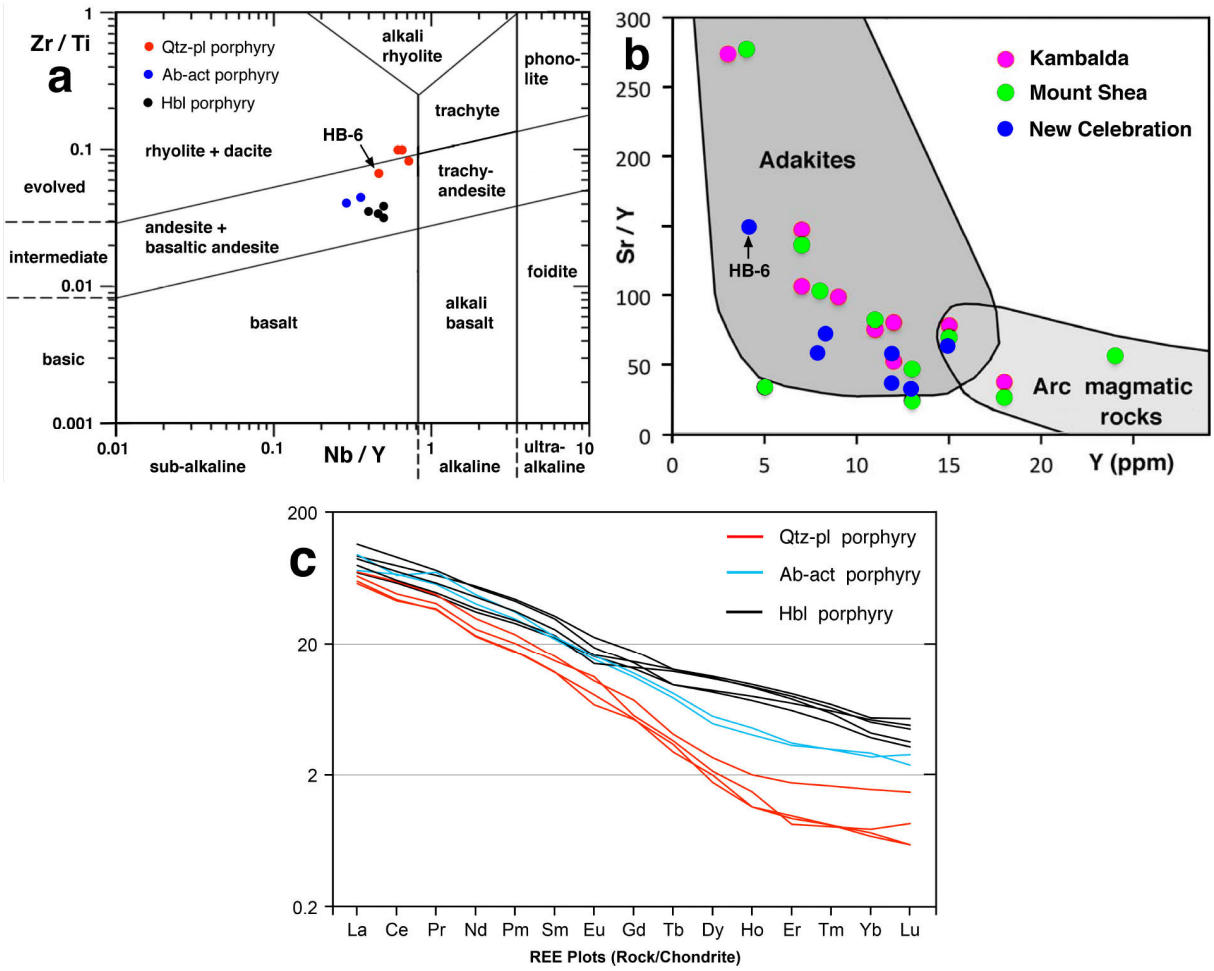

Figure 11. Classification of altered quartz-plagioclase (Qtz-pl) and albite-actinolite (Ab-act) altered porphyries from the New Celebration open pit (data in Table S1), and of hornblende (Hbl) porphyries from the wider mine area (samples 108834–108847 in [44]). (**a**) Pearce Zr/Ti versus Nb/Y diagram (after [41]) distinguishing calc–alkaline from alkaline series rocks. (**b**) Sr/Y versus yttrium adakite discrimination diagram for ca. 2660 Ma monzodiorite-suite porphyries in the Boulder Lefroy-Golden Mile fault system (modified from [5]). (**c**) Chondrite-normalized rare earth element (REE) diagram using the chondrite values in [45].

6.2. Younger Porphyry Suite (ca. 2660 Ma)

The new U-Pb zircon age, the high contents of TiO_2 (0.48–0.60 wt.%), Cr (130–131 ppm), Ni (52–63 ppm) and V (63–74 ppm), elevated Pt and Pd (6–7 ppb), and the REE-patterns (normalized La/Yb = 25–35; Table S1) link the albite-actinolite altered andesitic porphyries (Figure 11a) at New Celebration to the mantle-derived suite of monzodiorite-granodiorite-tonalite intrusions emplaced into the Boulder Lefroy-Golden Mile fault system at 2665–2655 Ma [5]. Some of the I-type porphyries contain zircon xenocrysts (2675–2685 Ma [5];) inherited from older calc-alkaline intrusions, probably because they used the same faults for ascent in the crust. The Albite-Actinolite Porphyry contains amphibolite xenoliths and partly resorbed granitoid (Figure 8c), perhaps the source of the

ca. 2800 Ma xenocryst. The andesitic "hornblende porphyries" in the New Celebration district [44] are also characterized by elevated TiO_2 (0.46–0.59 wt.%), Cr (288–435 ppm), Ni (96–211 ppm), V (114–176 ppm), Pt (2–3 ppb) and Pd (3–5 ppb) and represent less fractionated members of the monzodiorite suite (Figure 11b,c). They are not classified as "lamprophyres" [46] due to the presence of plagioclase phenocrysts (Figure 10c,d). The high-Cr-Ni-V and Sr/Y signature is typical of Neoarchean high-Mg sanukitoids [42], and of low-silica adakites derived as partial melts from metasomatized mantle peridotite in Cenozoic subduction zones [31].

6.3. Mg-Na Metasomatism

The Mg-number [$Mg/(Mg + Fe_{total})$] of least-altered sanukitoids in Canada decreases with increasing hornblende fractionation from 0.62 in monzodiorite to 0.43 in granodiorite [42], the latter close to the average (0.45) in TTG-batholiths. All porphyries at New Celebration have high Mg-numbers of 0.57–0.65 (Table S1). In the case of the older porphyries, this may be due to Mg-exchange with the host ultramafic schist. The replacement selvages of the Albite-Actinolite Porphyry, however, overprint the main-stage talc schist suggesting that the high Mg-numbers (0.62–0.65) reflect the dyke-centered sodic-calcic alteration. High Mg-numbers also characterize most monzodiorite-suite porphyries at Mt Shea (0.53–0.89 [10];) and at Kambalda (0.69–0.81 [9];). The Mg-enrichment is caused by the core to rim increase of Mg-Si relative to Fe-Al cations in igneous hornblende, a zonation related to crystallization under oxidizing conditions [9]. In addition, such hornblende contains up to 1.0 wt.% Cr_2O_3 [9]. At both locations, the partial replacement of hornblende by deuteric actinolite is widespread but minor, similar to that in least-altered monzodiorite/diorite at New Celebration (Figure 10c,d).

Another deuteric trend at Kambalda is the enrichment of sodium at constant aluminum. A benchmark for zoned igneous plagioclase (An27 to An10 [47];) is set by the stock of fractionated granodiorite-tonalite ($Na_2O/K_2O = 2.4$) emplaced into the dome-shaped D1 anticline at the town of Kambalda (Figure 1). Most porphyry dykes and sills including those well away from gold mineralization display pervasive albite alteration (An1–5). Even in large phenocrysts, the maximum anorthite content (An15) is more sodic than expected for dioritic plagioclase (An40 [9];). In dykes at Mt. Shea, the replacement of calcic plagioclase phenocrysts by porous albite-oligoclase (An3–18), disseminated clinozoisite and sericite is also widespread. The albite-rich groundmass contains minor fibrous actinolite, biotite-epidote aggregates, and rare replacement microcline in contact with epidote and chlorite [5].

6.4. The East Repulse Albitites

East Repulse is one of several ore bodies (112 t Au combined) constituting the Victory complex in the D3 Repulse thrust system at Kambalda [48]. The ore replaces amphibolite-facies magnesian meta-basalt and -komatiite at and below the main thrust, which offsets ca. 2660 Ma granodiorite-tonalite porphyry dykes crosscutting the folded greenstones [4]. Wall-rock alteration in meta-basalt/komatiite up to 200 m below the fault, most intense at dyke contacts, consists of early and late epidote bracketing main-stage biotite-amphibole-anhydrite-pyrite replacement and veining. In the porphyry dykes, fine-grained granular albite (An5) replaces most igneous plagioclase (An30). Pyrite, barite, celestine, and carbonate fill interstitial pores. Main-stage biotite-pyrite veins containing minor anhydrite, calcite, and trace electrum crosscut the porous albitite but are in turn overprinted by late-stage quartz-albite-carbonate-pyrite veins. Fluid temperature is estimated at 480 ± 60 °C based on the partitioning of fluorine between biotite and apatite [4]. The albitite dykes acted as conduits for ascending oxidized fluids, both sourced from the cupola of a dome-shaped granitoid pluton indicated by reflection seismic about 2 km below the deposit [49].

6.5. Dyke Emplacement at New Celebration

At the East Repulse deposit, albite alteration in porphyry dykes both pre- and post-dates main-stage gold mineralization but is part of the same hydrothermal event. At New Celebration, there is conflicting evidence with regard to time relationships. Although located about half way between the boudinaged Main Porphyry and the East Porphyry (Figure 4), the pervasive sodic-calcic alteration in the Albite-Actinolite Porphyry differs sharply from the sodic-potassic one in both adjacent dykes. Despite this difference, the porphyries share the same sulfide-oxide assemblage: pyrite ± chalcopyrite, magnetite, and late hematite. Two alternatives must be considered.

The Albite-Actinolite Porphyry was emplaced prior to main-stage gold mineralization, potential evidence includes: (1) large parts of the dyke were mined in the open pit at >1 g/t Au from the surface (+355 m) to about +300 m elevation; (2) actinolite in the dyke is selectively replaced by ankerite + phengite ± talc where sampled on the +267 m bench; (3) the Cr-Ni-V signature of sample HB-6 (11 g/t Au) suggests that andesitic dykes of the ca. 2660 Ma generation crosscut the Main Porphyry and constitute gold ore, although structural relations remain uncertain due to the sampling of blasted material on the pit floor.

Dyke emplacement was syn- to late-mineralization, evidence includes: (1) the low strain in the fractured dyke; (2) the intrusive contact crosscutting and the actinolite-pyrite selvage overprinting the foliation in main-stage talc-chlorite-dolomite ± phlogopite schist; (3) the Au-Ag-Bi-Se-Te signature of pyrite disseminated in the porphyry, which matches the signature of gold ore (Table 1); (4) very low gold grades (5 ppb; sample HB-8a) almost directly below high-grades (6.1 g/t; Figure 4) in drill holes; (5) the agreement between the estimated fluid temperature during sodic-calcic alteration in the dyke (300–350 °C) and main-stage gold mineralization (330 ± 20 °C).

As in the East Repulse deposit at Kambalda, these relationships suggest that the albite-actinolite alteration in the andesitic plagioclase porphyry was part of the hydrothermal system depositing gold at New Celebration. It is likely that late-stage dyke emplacement led to the preservation of the sodic-calcic assemblage within sodic-potassic alteration developed throughout the broad D2-D3 schist zone.

6.6. Gold-Related Albitites in Canada

Porphyry dykes in the Abitibi greenstone belt, Archean Superior Province, Canada, are also affected by pervasive, texture-destructive sodic-calcic alteration. The prevailing assemblage is albite-carbonate-chlorite-pyrite rather than albite-actinolite-pyrite but the whole-rock geochemistry is similar (Table 2). The metasomatic calcic component is represented by carbonate. Given the alteration overprint, the igneous parentage of the Canadian albitites is controversial. Most geochemical data suggest a precursor of calc-alkaline andesitic/dioritic composition [2,50].

In subsidiary shear zones north of the regional Larder Lake-Cadillac fault zone, albitites occur in the Francoeur (21 t Au) and Kiena deposits (48 t Au). At Francoeur, weakly strained red dykes were emplaced into the shear zone during low-grade muscovite-hematite-pyrite alteration preceding main-stage albite-carbonate-pyrite replacement and late carbonate-gypsum ± anhydrite ± hematite veining [51]. At Kiena, mineralization is centered on a funnel-shaped albitite dyke swarm crosscut by "intermineral" granodiorite-tonalite and plagioclase porphyry, which enclose xenoliths of main-stage gold ore but are in turn crosscut by late auriferous quartz-carbonate-pyrite veins. The U-Pb zircon age of the granodiorite dyke constrains gold mineralization to 2686 ± 2 Ma [52].

Similar dyke-ore relationships occur in the Kerr Addison-Chesterville deposit (336 t Au) hosted by muscovite-carbonate-albite-altered, schistose meta-komatiite and amphibolite in the main branch of the Larder Lake-Cadillac Fault [2]. Albitite dykes 0.3–2 m thick are confined to the green fuchsite-dolomite alteration envelope of the ore, which narrows from 900 m length and 50–60 m width near the surface to 300 × 25–50 m at 1700 m depth, forming a flat funnel-shaped zone marked by 5–15 vol.% albitite. The dykes are subdivided into early- (A1), main- (A2), and late-stage (A3) relative to gold mineralization

(Table 2) based on crosscutting relationships and wall-rock xenoliths including fragments of auriferous veins. Most plot in the calc-alkaline andesite field of the Zr/TiO_2 versus Nb/Y diagram [2]. Some A1-dykes are spotted pink and contain minor anhydrite. The dyke swarm plunges steeply east and converges towards the Chesterville Plug, a lens-shaped intrusion 40 × 120 m in plan section, which is continuous from 180 m to 2000 m depth [2,53].

Table 2. Whole-rock analyses of albitite dykes in the New Celebration (NC), Hollinger-McIntyre (H-McI), and Kerr Addison-Chesterville (KA-Ch) gold deposits.

Deposit	**NC**	**H-McI**	**KA-Ch**	**KA-Ch**
Sample no.	HB-8a	194	88.31 (A2)	88.83 (A3)
Mineralogy	ab-act-cb	ab-cb-chl	ab-cb-chl	ab-cb-chl-pg
SiO_2 (wt.%)	61.69	47.70	44.80	44.40
TiO_2	0.48	0.55	0.57	0.75
Al_2O_3	15.17	11.60	10.80	10.90
Fe_2O_3	3.83	6.61	6.41	8.78
MnO	0.05	0.14	0.10	0.15
MgO	3.13	7.42	10.40	8.65
CaO	3.90	7.98	8.41	7.54
Na_2O	8.92	3.55	3.29	4.04
K_2O	0.08	0.41	0.33	0.61
P_2O_5	0.28	0.26	0.37	0.43
H_2O	0.12	2.10	2.60	2.60
CO_2	1.43	11.50	12.10	11.00
Sulfur	1.06	0.07	0.07	0.56
Total	100.14	99.89	100.25	100.41
Au (ppb)	5	n.a.	25	490
Ag	50	n.a.	<10	30
Cr (ppm)	130	601	n.a.	n.a.
Ni	63	128	n.a.	n.a.
V	74	174	n.a.	n.a.
Nb	3	11	5	7
Y	8	14	13	20
Zr	127	151	104	123

Data sources: NC (Table S1), H-McI [1], KA-Ch [2]. Minerals: albite (ab), actinolite (act), carbonate (cb), chlorite (chl), paragonite (pg). Not analyzed (n.a.).

In the giant Hollinger-McIntyre deposit (986 t Au) north of the Destor-Porcupine Fault, albitite dykes 0.3–5 m thick and up to 600 m long crosscut foliated and lineated stocks of quartz-plagioclase porphyry, which in turn crosscut a succession of folded, greenschist-facies Mg- and Fe-tholeiitic flows. The U-Pb zircon ages of the strained quartz-plagioclase porphyries vary from 2691 ± 3 Ma to 2688 ± 2 Ma, whereas the albitite dykes are dated at 2673 +6/−2 Ma [54]. The albitites have a distinct high-Mg-Cr-Ni signature (Table 2), contain biotite phenocrysts and chlorite-rutile pseudomorphs after hornblende, and enclose rounded xenoliths (1–30 cm) of sodic microgranite [1].

The Hollinger-McIntyre deposit comprises (1) porphyry-hosted Cu-Au-Ag ± Mo ore (10 Mt at 0.67% Cu, 0.59 g/t Au, 2.93 g/t Ag; 1963–1982) and (2) the main system of gold- and scheelite-bearing quartz-carbonate-pyrite veins, both close but spatially separated [1,55]. The Cu-Au ore forms pipe-shaped shoots within a 450 × 150 m pink anhydrite-chlorite (± carbonate-tourmaline) zone extending from 180 to >1400 m depth. Stage 1 chalcopyrite, molybdenite, and trace hessite are co-genetic with anhydrite and hematite in the low-grade outer zone (0.16–0.35% Cu; 0.04–0.05% Mo). The early anhydrite is overprinted by central grey albite and later sericite ± K-feldspar alteration, the albite associated with Stage 2 bornite ± chalcocite-gold-petzite mineralization [1]. The sericitic zones contain 10-60 vol.% quartz-anhydrite-carbonate-chalcopyrite veins, disseminated Stage 3 chalcopyrite + pyrite + native gold, and Stage 4 molybdenite, galena, sphalerite, and tetrahedrite with inclusions of amalgam and electrum [1]. The age of the Cu-Au-Ag

zone is constrained by molybdenite Re-Os data from drill hole MC03-12, which intersected chalcopyrite ore at 330 m depth. Two samples rich in radiogenic ^{187}Os (>2500 ppb) gave a weighted mean Re-Os model age of 2672 ± 7 Ma [56,57], identical within error with the U-Pb age of the albitite dykes. While geochronology and shared sodium metasomatism link dyke emplacement to the formation of the Cu-Au-Ag zone, the age of the main gold-quartz vein system (Au/Ag = 5:1) remains uncertain. As quartz-tourmaline and -carbonate veins crosscut the albitites, the vein system must be younger [50].

6.7. Syenite-Associated Gold Deposits

In the Abitibi greenstone belt, albite-dolomite altered disseminated gold deposits associated with late-orogenic quartz monzonite-syenite stocks and dykes are distinguished as a separate intrusion-related group [58]. The deposits consist of pyritic quartz veinlet stockworks enriched in Cu (up to 0.6 wt.%), As, Te and, less commonly, in Mo, W, Zn, and Pb. They are characterized by intense ore-grade albite replacement (>8 wt.% Na_2O in syenite), by the oxidized assemblage hematite-magnetite ± anhydrite, and by pyrite with negative $\delta^{34}S$ values [58]. In the Boulder Lefroy-Golden Mile fault system, the syenite association is rare but represented by the small (2.9 t Au) Bellerophon Au-Te deposit at Kambalda [48,59]. The genetic relationship between the calc-alkaline monzodiorite and the alkaline monzonite-syenite intrusive suites, both associated with oxidized gold deposits, is not fully understood.

In the Larder Lake-Cadillac Fault, southern Abitibi Belt, clinopyroxenite, hornblendite, diorite and monzodiorite form cumulate border phases in the syenitic Murdock Creek pluton [60]. In the nearby Kirkland Lake district, the site of a giant Au-Te-Mo deposit (750 t Au), hornblende quartz monzodiorite crosscuts augite syenite [61,62]. The main minerals in the syenites are diopsidic augite, Ti-rich biotite, perthitic K-feldspar, and minor plagioclase (An30–34) in less differentiated phases. Classic alkaline indicator minerals such as nepheline, leucite, aegirine and igneous sodic amphibole are rare or absent. The high Mg-numbers of augite (0.72–0.88), magnetite rimmed by hematite or titanite, and the absence of ilmenite indicate a high magmatic oxidation state, whereas the predominance of augite suggests a low water content during melt crystallization [60]. While minor deuteric sodium enrichment is present [60], there is little evidence that alkali feldspar syenite evolved to form the albitites discussed above. The average Abitibi syenite [30] contains lower TiO_2 (0.26 wt.%), Cr (42 ppm), Ni (43 ppm), and V (39 ppm) than the dykes listed in Table 2.

7. Summary and Conclusions

1. In the Boulder Lefroy-Golden Mile fault system (>2300 t Au), eastern Yilgarn Craton, Western Australia, hematite- and anhydrite-bearing mesothermal gold deposits such as the Golden Mile and New Celebration are associated in space and time with I-type monzodiorite-suite intrusions of adakitic affinity (high Mg, Cr, Ni, V; elevated Pt, Pd). In regional faults of the Abitibi greenstone belt, Canada, this association is evident in the Hollinger-McIntyre and Kerr Addison-Chesterville deposits.
2. In the fault zones, mesothermal gold deposits are locally associated with Cu-Au-Ag deposits, such as the epidote-magnetite endoskarns at Mt Shea southeast of Kalgoorlie, Western Australia, and the sericite-albite-anhydrite ore bodies in the McIntyre mine at Timmins, Canada.
3. Diagnostic features of gold-related monzodiorite-suite intrusions are the Mg-enrichment due to hornblende crystallization under oxidizing conditions, and the deuteric replacement of hornblende by actinolite and of calcic plagioclase by albite. The end member hydrothermal product of this process may be the pervasive albitization of distal porphyry dykes (albitites), represented by albite-actinolite-pyrite assemblages at New Celebration, and by albite-carbonate-chlorite-pyrite assemblages at Hollinger-McIntyre and Kerr Addison-Chesterville.
4. Albitite dykes are an integral part of the hydrothermal systems at Francoeur, Kiena, Kerr Addison-Chesterville and Hollinger-McIntyre in Canada, and at East Repulse

and New Celebration in Western Australia. The "intermineral" dyke relationships in this diverse group of deposits provide evidence that ore formation at New Celebration took place during the emplacement of the Albite-Actinolite Porphyry at 2662 ± 4 Ma. Just as their syenite-associated counterparts, oxidized monzodiorite-associated gold deposits must be classified as intrusion-related, distinct from those interpreted as "orogenic".

5. Absolute and relative age constraints in the Boulder Lefroy-Golden Mile fault system are as follows. Gold mineralization at ca. 2660 Ma at New Celebration (this study) and in the Golden Mile [11] was coincident with the transition from D2 sinistral strike-slip to D3 reverse faulting. At Mt Shea and at Kambalda, where reverse faults control Fe-Cu-Au endoskarns and mesothermal gold ore bodies, respectively, D3 faulting was broadly synchronous with the emplacement of monzodiorite-suite porphyries dated at 2662 ± 6 Ma to 2658 ± 4 Ma [5].

Supplementary Materials: The following data are available online at https://www.mdpi.com/article/10.3390/min11111288/s1, Figure S1: Scanning electron microscope backscattered electron and cathodo-luminescence images of SHRIMP mount 12-21C showing igneous zircons with oscillatory zones and alteration titanite (Ttn) from porphyry HB-8a. Table S1a: Whole rock major element analyses and Mesonorms of porphyry dykes from the Hampton–Boulder open pit and outcrops at the New Celebration gold deposit, Kalgoorlie, Western Australia. Table S1b: Whole rock trace element analyses of porphyry dykes from the Hampton Boulder open pit and outcrops at the New Celebration deposit. Table S2: Energy dispersive electron microprobe analyses of actinolite and albite in dykes from the Hampton Boulder open pit, New Celebration deposit. Table S3: SHRIMP ion microprobe U-Pb analyses of zircons from the Albite-Actinolite Porphyry (sample HB-8a), Hampton-Boulder open pit, New Celebration gold deposit, Kalgoorlie, Western Australia.

Author Contributions: Conceptualization, A.G.M.; methodology, A.G.M.; validation, A.G.M., N.J.M. and J.R.M.; formal analysis, A.G.M., N.J.M. and J.R.M.; investigation, A.G.M.; resources, A.G.M., N.J.M. and J.R.M.; data curation, A.G.M.; writing—original draft preparation, A.G.M.; writing—review and editing, A.G.M.; visualization, A.G.M.; supervisoon, A.G.M.; project administration, A.G.M. All authors have read and agreed to the published version of the manuscript.

Funding: This research received no external funding.

Data Availability Statement: All data are publicly available in the Supplementary Materials.

Acknowledgments: The senior author is grateful to Mark Cossom of Dioro South Kalgoorlie Operations, who arranged access and sampling in the New Celebration open pit in July 2008, about 9 months before the collapse of the eastern pit wall buried all exposures. Neal McNaughton acknowledges support from the John de Laeter Center at Curtin University for access to the SHRIMP II facility, and Janet Muhling support from the Centre for Microscopy, Characterisation and Analysis (CMCA) at the University of Western Australia for access to the TESCAN scanning electron microscope. Critical comments by three anonymous referees helped to improve the manuscript considerably.

Conflicts of Interest: The authors declare no conflict of interest.

References

1. Burrows, D.R.; Spooner, E.T.C. The McIntyre Cu-Au deposit, Timmins, Ontario, Canada. In *Proceedings of Gold'86, an International Symposium on the Geology of Gold*; Macdonald, A.J., Ed.; Gold'86: Toronto, ON, Canada, 1986; pp. 23–39.
2. Smith, J.P.; Spooner, E.T.C.; Broughton, D.W.; Ploeger, F.R. *Archean Au-Ag-(W) Quartz Vein/Disseminated Mineralisation within the Larder Lake-Cadillac Break, Kerr Addison-Chesterville System, North East Ontario, Canada*; Open File Rep. 5831; Ontario Geoscience Research Grant Program, Grant no. 364; Ontario Geological Survey: Sudbury, ON, Canada, 1993; 310p.
3. Dubé, B.; Mercier-Langevin, P.; Ayer, J.; Pilote, J.-L.; Monecke, T. Gold deposits of the world-class Timmins-Porcupine Camp, Abitibi greenstone belt, Canada. *SEG Spec. Publ.* **2020**, *23*, 53–80.
4. Bath, L.B.; Walshe, J.L.; Cloutier, J.; Verrall, M.; Cleverley, J.S.; Pownceby, M.I.; Macrae, C.M.; Wilson, N.C.; Tunjic, J.; Nortje, G.S.; et al. Biotite and apatite as tools for tracking pathways of oxidized fluids in the Archean East Repulse gold deposit, Australia. *Econ. Geol.* **2013**, *108*, 667–690. [CrossRef]

5. Mueller, A.G.; Hagemann, S.G.; McNaughton, N.J. Neoarchean orogenic, magmatic and hydrothermal events in the Kalgoorlie-Kambalda area, Western Australia: Constraints on gold mineralization in the Boulder Lefroy–Golden Mile fault system. *Miner. Depos.* **2020**, *55*, 633–663. [CrossRef]
6. Norris, N.D. New Celebration gold deposits. In *Geology of Mineral Deposits of Australia and Papua New Guinea*; Monograph 14; Hughes, F.E., Ed.; Australasian Institute of Mining and Metallurgy: Melbourne, Australia, 1990; pp. 449–454.
7. Cassidy, K.F.; Champion, D.C.; Krapez, B.; Barley, M.E.; Brown, S.J.A.; Blewett, R.S.; Groenewald, P.B.; Tyler, I.M. *A Revised Geological Framework for the Yilgarn Craton, Western Australia*; Record 2006/8; Geological Survey of Western Australia: Perth, Australia, 2006; 8p.
8. Tripp, G.I. *Stratigraphy and Structure in the Neoarchaean of the Kalgoorlie District, Australia: Critical Controls on Greenstone-Hosted Gold Deposits*; Report 199; Geological Survey of Western Australia: Perth, Australia, 2019; 475p.
9. Perring, C.S.; Rock, N.M.S. Relationships between calc-alkaline acidic and basic (mantle-derived) magmas in Late Archaean composite dykes, Kambalda Goldfield, Western Australia. *Prec. Res.* **1991**, *52*, 245–273. [CrossRef]
10. Mueller, A.G. Copper-gold endoskarns and high-Mg monzodiorite-tonalite intrusions at Mt. Shea, Kalgoorlie, Australia: Implications for the origin of gold-pyrite-tennantite mineralization in the Golden Mile. *Miner. Depos.* **2007**, *42*, 737–769. [CrossRef]
11. Gauthier, L.; Hagemann, S.; Robert, F. The geological setting of the Golden Mile gold deposit, Kalgoorlie, WA. In *Kalgoorlie 2007, Old Ground, New Knowledge, Abstracts*; Record 2007/14; Bierlein, F.P., Knox-Robinson, C.M., Eds.; Geoscience Australia: Canberra, Australia, 2007; pp. 181–185.
12. Mueller, A.G. Structural setting of Fimiston- and Oroya-style pyrite-telluride-gold lodes, Paringa South mine, Golden Mile, Kalgoorlie: 1. Shear zone systems, porphyry dykes and deposit-scale alteration zones. *Miner. Depos.* **2020**, *55*, 665–695. [CrossRef]
13. Mueller, A.G.; Lawrance, L.M.; Muhling, J.; Pooley, G.D. Mineralogy and PTX relationships of the Archean Hannan South Au-Cu (Co-Bi) deposit, Kalgoorlie, Western Australia: Thermodynamic constraints on the formation of a zoned intrusion-related skarn. *Econ. Geol.* **2012**, *107*, 1–24. [CrossRef]
14. Vanderhor, F.; Groves, D.I. *Systematic Documentation of Archaean Gold Deposits of the Yilgarn Block*; Report 193; Minerals Energy Res. Inst. Western Australia (MERIWA): Perth, Australia, 1998.
15. Langsford, N. The stratigraphy of Locations 48 and 50. In *The 1989 Kalgoorlie Gold Workshop—Annual Conference and Eastern Goldfields Geological Discussion Group, Kalgoorlie, Western Australia*; Glacken, I.M., Ed.; Australian Institute of Mining and Metallurgy: Melbourne, Australia, 1989; pp. B1–B8.
16. Dielemans, P. Structural Controls on Gold Mineralization in the Southern Ore Zone of the Hampton Boulder Deposit, New Celebration Gold Mine, Western Australia. Ph.D. Thesis, the University of Western Australia, Perth, Australia, 2000.
17. Weinberg, R.F.; van der Borgh, P.; Bateman, R.J.; Groves, D.I. Kinematic history of the Boulder-Lefroy shear zone system and controls on associated gold mineralization, Yilgarn Craton, Western Australia. *Econ. Geol.* **2005**, *100*, 1407–1426. [CrossRef]
18. Nichols, S.J.; Hagemann, S.G. Structural and hydrothermal alteration evidence for two gold mineralization events at the New Celebration gold deposits in Western Australia. *Aust. J. Earth Sci.* **2014**, *61*, 113–141. [CrossRef]
19. Copeland, I.K.; Geological Staff New Hampton Goldfield, N.L. Jubilee gold deposit, Kambalda. In *Geology of Australian and Papua New Giunean Mineral Deposits*; Monograph 22; Berkman, D.A., Mackenzie, D.H., Eds.; Australian Institute of Mining and Metallurgy: Melbourne, Australia, 1998; pp. 219–224.
20. Honman, C.S. *The Geology of the Country to the South of Kalgoorlie Including the Mining Centres of Golden Ridge and Feysville*; Bulletin 66; Geological Survey of Western Australia: Perth, Australia, 1916; p. 63.
21. Mikucki, E.J.; Roberts, F.I. *Metamorphic Petrography of the Kalgoorlie Region, Eastern Goldfields Granite-Greenstone Terrane: METPET Database*; Record 2003/12; Geological Survey of Western Australia: Perth, Australia, 2004; 40p.
22. Williams, H. The Lithological Setting and Controls on Gold Mineralization in the Southern Ore Zone of the Hampton Boulder Gold Deposit, New Celebration Gold Mine, Western Australia. B.Sc. Honours Thesis, The University of Western Australia, Perth, Australia, 1994.
23. Hodkiewicz, P.F.; Groves, D.I.; Davidson, G.J.; Weinberg, R.F.; Hagemann, S.G. Influence on structural setting on sulphur isotopes in Archean orogenic gold deposits, Eastern Goldfields Province, Yilgarn, Western Australia. *Miner. Depos.* **2009**, *44*, 129–150. [CrossRef]
24. Rye, R.O. The evolution of magmatic fluids in the epithermal environment: The stable isotope perspective. *Econ. Geol.* **1993**, *88*, 733–753. [CrossRef]
25. Massonne, H.-J.; Schreyer, W. Phengite geobarometry based on the limiting assemblage with K-feldspar, phlogopite, and quartz. *Contrib. Mineral. Petrol.* **1987**, *96*, 212–224. [CrossRef]
26. Tröger, W.E. *Optische Bestimmung der Gesteinsbildenden Minerale. Teil 1 Bestimmungstabellen*, 4th ed.; Schweizerbart'sche Verlagsbuchhandlung: Stuttgart, Germany, 1971; 188p. (In German)
27. Ramdohr, P. *Die Erzmineralien und Ihre Verwachsungen*; Akademie Verlag: Berlin, Germany, 1975; 1277p. (In German)
28. Spry, P.G.; Gedlinske, B.L. *Tables for the Determination of Common Opaque Minerals*; Society of Economic Geologists: Littleton, CO, USA, 1987; 52p.
29. O'Beirne, W.R. The Acid Porphyries and Porphyroid Rocks of the Kalgoorlie Area. Ph.D. Thesis, The University of Western Australia, Perth, Australia, 1968.

30. Feng, R.; Fan, J.; Kerrich, R. Noble metal abundances and characteristics of six granitic magma series, Archean Abitibi Belt, Pontiac Subprovince: Relationships to metallogeny and overprinting of mesothermal gold deposits. *Econ. Geol.* **1993**, *88*, 1376–1401. [CrossRef]
31. Martin, H.; Smithies, R.H.; Rapp, R.; Moyen, J.F.; Champion, D. An overview of adakite, tonalite-trondhjemite-granodiorite (TTG), and sanukitoid: Relationships and some implications for crustal evolution. *Lithos* **2005**, *79*, 1–24. [CrossRef]
32. Krauskopf, K.B.; Bird, D.K. *Introduction to Geochemistry*, 3rd ed.; McGraw-Hill: Boston, MA, USA, 1995; 647p.
33. Barth, T.F.W. Principles of classification and norm calculations of metamorphic rocks. *J. Geol.* **1959**, *67*, 135–152. [CrossRef]
34. Holland, T.J.B.; Blundy, J. Non-ideal interactions in calcic amphiboles and their bearing on amphibole-plagioclase thermometry. *Contrib. Mineral. Petrol.* **1994**, *116*, 433–447. [CrossRef]
35. Holland, T.J.B.; Powell, R. A Program to Calculate Activities of Mineral End Members from Chemical Analyses Usually Determined by Electron Microprobe. Available online: https://www.esc.cam.ac.uk/astaff/holland/ax.html (accessed on 24 February 2019).
36. Williams, I.S. U-Th-Pb geochronology by ion microprobe. *Rev. Econ. Geol.* **1998**, *7*, 1–35.
37. Ludwig, K.R. *User's Manual for Isoplot 3.75: A Geochronological Toolkit for Microsoft Excel*; Special Publ. no. 5; Berkeley Geochronology Center, Berkeley University: San Francisco, CA, USA, 2012; 75p.
38. Cullen, I.; Norris, N. Gold deposits of the New Celebration gold mine. In *Western Australian Gold Deposits: Bicentennial Gold 88 Excursion Guidebook*; Publ. 14; Groves, D.I., Barley, M.E., Ho, S.E., Hopkins, G.M.F., Eds.; The University of Western Australia: Perth, Australia, 1988; pp. 87–90.
39. Leake, B.E.; Woolley, A.R.; Arps, C.E.S.; Birch, W.D.; Gilbert, M.C.; Grice, J.D.; Hawthorne, F.C.; Kato, A.; Kisch, H.J.; Krivovichev, V.G.; et al. (IMA) Nomenclature of amphiboles: Report of the subcommittee on amphiboles of the International Mineralogical Association, Commission on new minerals and mineral names. *Can. Mineral.* **1997**, *35*, 219–246.
40. Spear, F.S. NaSi = CaAl exchange equilibrium between plagioclase and amphibole. *Contrib. Mineral. Petrol.* **1980**, *72*, 33–41. [CrossRef]
41. Pearce, J.A. A user's guide to basalt discrimination diagrams. In *Trace Element Geochemistry of Volcanic Rocks: Applications for Massive Sulphide Exploration*; Short Course Notes 12; Wyman, D.A., Ed.; Geological Association of Canada: St. John's, NL, Canada, 1996; pp. 79–113.
42. Stern, R.A.; Hanson, G.N. Archean high-Mg granodiorite: A derivative of light rare earth element-enriched monzodiorite of mantle origin. *J. Petrol.* **1991**, *32*, 201–238. [CrossRef]
43. Cassidy, K.F.; Barley, M.E.; Groves, D.I.; Perring, C.S.; Hallberg, J.A. An overview of the nature, distribution and inferred tectonic setting of granitoids in the late-Archaean Norseman-Wiluna Belt. *Prec. Res.* **1991**, *51*, 51–83. [CrossRef]
44. Taylor, W.R.; Rock, N.M.S.; Groves, D.I.; Perring, C.S. Geochemistry of Archean shoshonitic lamprophyres from the Yilgarn Block, Western Australia: Au abundance and association with gold mineralization. *Appl. Geochem.* **1994**, *9*, 197–222. [CrossRef]
45. Nakamura, N. Determination of REE, Ba, Mg, Na and K in carbonaceous and ordinary chondrites. *Geochim. Cosmochim. Acta* **1974**, *38*, 757–775. [CrossRef]
46. Streckeisen, A. Classification and nomenclature of volcanic rocks, lamprophyres, carbonatites, and melilitic rocks: Recommendations and suggestions of the IUGS subcommission on the systematics of igneous rocks. *Geology* **1979**, *7*, 331–335. [CrossRef]
47. Roddick, J.C.M. Responses of Strontium Isotopes to Some Crustal Processes. Ph.D. Thesis, Australian National University, Canberra, Australia, 1974.
48. Oxenburgh, S.K.; Falconer, M.; Doutch, D.; Edmonds, P.; Foley, A.; Jane, M. Kambalda-St Ives goldfield. In *Australian Ore Deposits*; Monograph 32; Phillips, G.N., Ed.; Australian Institute of Mining and Metallurgy: Melbourne, Australia, 2017; pp. 215–222.
49. Blewett, R.S.; Squire, R.; Miller, J.M.; Henson, P.A.; Champion, D.C. Architecture and geodynamic evolution of the St Ives Goldfield, eastern Yilgarn Craton, Western Australia. *Prec. Res.* **2010**, *183*, 275–291. [CrossRef]
50. Burrows, D.R.; Spooner, E.T.C.; Wood, P.C.; Jemielita, R.A. Structural controls on formation of the Hollinger-McIntyre Au quartz vein system in the Hollinger Shear Zone, Timmins, southern Abitibi greenstone belt, Ontario. *Econ. Geol.* **1993**, *88*, 1643–1663. [CrossRef]
51. Couture, J.F.; Pilote, P. The geology and alteration patterns of a disseminated shear zone-hosted mesothermal gold deposit: The Francoeur 3 deposit, Rouyn-Noranda, Quebec. *Econ. Geol.* **1993**, *88*, 1664–1684. [CrossRef]
52. Morasse, S.; Wasteneys, H.A.; Cormier, M.; Helmstaedt, H.; Mason, R. A pre-2686 Ma intrusion-related gold deposit at the Kiena mine, Val d'Or, Quebec, southern Abitibi subprovince. *Econ. Geol.* **1995**, *90*, 1310–1321. [CrossRef]
53. Spooner, E.T.C. Magmatic sulphide/volatile interaction as a mechanism for producing chalcophile element enriched, Archean Au-quartz, epitjermal Au-Ag and Au skarn hydrothermal ore fluids. *Ore Geol. Rev.* **1993**, *7*, 359–379. [CrossRef]
54. Corfu, F.; Krogh, T.E.; Kwok, Y.Y.; Jensen, L.S. U-Pb zircon geochronology in the southwestern Abitibi greenstone belt, Superior Province. *Can. J. Earth Sci.* **1989**, *26*, 1747–1763. [CrossRef]
55. Wood, P.C.; Burrows, D.R.; Thomas, A.V.; Spooner, E.T.C. The Hollinger-McIntyre Au-quartz vein system, Timmins, Ontario, Canada: Geologic characteristics, fluid properties and light stable isotope geochemistry. In *Proceedings of Gold'86, an International Symposium on the Geology of Gold*; Macdonald, A.J., Ed.; Gold'86: Toronto, ON, Canada, 1986; pp. 56–80.
56. Hall, G.; Placer Dome Asia Pacific, Perth, Western Australia, Australia. Personal communication: Drill hole location of molybdenite samples from the McIntyre Cu-Au ore body dated by the Re-Os method, 2003.

57. Bateman, R.; Ayer, J.A.; Dubé, B.; Hamilton, M.A. *The Timmins-Porcupine Gold Camp, Northern Ontario: The Anatomy of an Archaean Greenstone Belt and Its Gold Mineralization*; Open File Report 6158; Discover Abitibi Initiative; Ontario Geological Survey: Sudbury, ON, Canada, 2005; 90p.
58. Robert, F. Syenite-associated disseminated gold deposits in the Abitibi greenstone belt, Canada. *Miner. Depos.* **2001**, *36*, 503–516. [CrossRef]
59. Xue, Y.; Campbell, I. The mineralogy of the Bellerophon-Nelson telluride-bearing gold deposit, St. Ives Camp, Yilgarn Craton, Western Australia. *Can. Mineral.* **2014**, *52*, 981–1006. [CrossRef]
60. Rowins, S.M.; Lalonde, A.E.; Cameron, E.M. Magmatic oxidation in syenitic Murdock Creek intrusion, Kirkland Lake, Ontario: Evidence from the ferromagnesian silicates. *J. Geol.* **1991**, *99*, 395–414. [CrossRef]
61. Hicks, K.D.; Hattori, K. Grant 313: Magmatic-hydrothermal and wall rock alteration petrology at the Lake Shore gold deposit, Krikland Lake, Ontario. *Ontario Geol. Surv. Misc. Pap.* **1988**, *140*, 192–204.
62. Hattori, K.; Levesque, G. Grant 313: Hydrothermal activity in the Kirkland Lake intrusive complex. *Ontario Geol. Surv. Misc. Pap.* **1989**, *143*, 59–67.